Title:

Evolution of gastrointestinal tract morphology and plasticity in cave-adapted Mexican tetra, *Astyanax mexicanus*

Authors:

Misty R. Riddle[1], Fleur Damen[1], Ariel Aspiras[1,*], Julius A. Tabin[1], Suzanne McGaugh[2], Clifford J. Tabin[1,#]

Affiliations:

1. Department of Genetics, Blavatnik Institute, Harvard Medical School, Boston, MA 02115
2. Ecology, Evolution, and Behavior, University of Minnesota, Saint Paul, MN

* Current affiliation: Department of Stem Cell and Regenerative Biology, Harvard University, Cambridge, MA 02138

\# For correspondence: tabin@genetics.med.harvard.edu

Abstract

The gastrointestinal tract has evolved in numerous ways to allow animals to optimally assimilate energy from different foods. The morphology and physiology of the gut is plastic and can be greatly altered by diet in some animals. In this study, we investigated the evolution and plasticity of gastrointestinal tract morphology by comparing laboratory-raised cave- and river-adapted forms of the Mexican tetra, *Astyanax mexicanus,* reared under different dietary conditions. In the wild, river-dwelling populations (surface fish) consume plants and insects throughout the year, while cave-dwelling populations (cavefish) live in a perpetually dark environment and depend on nutrient-poor food brought in by bats or seasonal floods. We found that multiple cave populations converged on a reduced number of digestive appendages called pyloric caeca and that some cave populations have a lengthened gut while others have a shortened gut. Moreover, we identified differences in how gut morphology and proliferation respond to diet between surface fish and cavefish. Using a combination of quantitative genetic mapping, population genetics, and RNA sequencing, we found that changes to the molecular and genetic pathways that influence cell proliferation, differentiation, and immune system function may underlie evolution of the cavefish gut.

Introduction

The gastrointestinal tract consists of functional regions distinguished by the organization of muscle and mucosal layers and cellular composition of epithelium lining the lumen. The secretory and absorptive cell types of the epithelium are constantly being replaced by self-renewing stem cells. Gut homeostasis requires integration of intrinsic signaling pathways set up during development, with external cues. For example, in the mammalian gut, Notch and WNT signaling is essential for establishing the stem cell niche and balancing stem cell renewal and differentiation of cell types (reviewed in 1). High-fat diet alters these pathways to favor self-renewal and secretory cell formation (2, 3). Cytokine signals from tissue-resident immune cells can also promote stem cell renewal in response to infection (4, 5). While studies utilizing model organisms and organoid culture have begun to reveal how homeostasis of the epithelium is maintained, there is a limited understanding of how these pathways evolve as animals adapt to different diets.

Evolutionary changes to gut morphology, such as expansion of functional domains, have been correlated to altered patterns of gene expression during development (6). The organization of the gut epithelium into crypts that support villi is important for stem cell maintenance in mammals, but in other species the epithelium is characterized by irregular folds, zig-zags, honeycomb patterns, or a spiral fold (7, 8). The presence of spatially restricted gut stem cells is common across distant phyla (i.e. arthropods and chordates) (9–11). Although it has been demonstrated that diet influences gut morphology in a number of species (reviewed in 12), evolution of the signaling pathways that integrate internal and external cues is not well understood. For animals that survive months without food, like snakes and migrating birds (13–15), altering the pathways that control homeostasis of the epithelium was likely critical to balance nutrient assimilation and energy conservation.

Astyanax mexicanus is a species of fish that exists as river- and cave-adapted populations that evolved on very different diets (16, 17). The river (surface) fish have access to insects and plants in abundance, while the cavefish are dependent on predominantly bat droppings and material brought in by seasonal floods (16, 17). There are a number of cave populations, named for the caves they inhabit (i.e. Tinaja, Pachón, Molino). Based on whole genome sequencing analysis, these populations reflect two independent cave derivations from surface fish within the last 200,000 years; Tinaja and

Pachón cavefish populations form a separate clade from Molino cavefish (18). Cavefish have converged on similar morphological changes, such as eye loss and increased sensory structures (19–21), behavioral changes such as reduced sleep (22–25), and metabolic changes such as increased fat accumulation and starvation resistance (26–28). We previously showed that Pachón cavefish have altered gastrointestinal motility during post-larval growth to slow food transit, possibly to achieve increased nutrient absorption (29).

In this study, we explore whether cave-adaptation has led to changes in the adult gut. First, we describe the anatomy and histology of the *A. mexicanus* gastrointestinal tract, noting distinct functional regions. Second, we compare *A. mexicanus* surface and cave populations fed the same diet and discover differences in pyloric caeca number and gut length. We show that the homeostasis and morphology of the gut responds differently to changes in diet comparing Tinaja cavefish to surface fish. To investigate the genetic architecture controlling gut length, we carry out a Quantitative Trait Locus (QTL) analysis, and identify a significant QTL associated with hindgut length. We examine genes within the QTL using population genetics and RNA sequencing and reveal genetic pathways that have been altered during the evolution of gut morphology in *A. mexicanus*.

Results

Anatomy and histology of the adult Astyanax mexicanus gastrointestinal (GI) tract

The GI tract of teleost fish is commonly divided into four sections from anterior to posterior: head gut, foregut, midgut, and hindgut. These sections are easily defined in *A. mexicanus* and can be further subdivided based on distinct morphology and histology. The foregut consists of the esophagus, stomach, and pylorus (Figure 1A, B). The esophagus has two perpendicular layers of striated muscle and a stratified epithelium of mucus secreting cells, identifiable by a lack of staining with hematoxylin and eosin (Figure 1A). It connects to the J-shaped stomach that has three muscle layers: outermost longitudinal, the middle and thickest circumferential, and innermost oblique (Figure 1B). Gastric glands are evident in the stomach mucosa; at the base of the glands, pepsin-secreting chief cells are distinguishable by eosinophilic granules. The lumen-facing epithelium of the stomach

consists of columnar mucus-secreting cells. The stomach ends at the pylorus that has thick muscle layers and connects the foregut to the midgut.

The midgut is the longest portion of the GI tract. The proximal end of the midgut contains pyloric caeca: pouch structures that have a thin layer of outer connective tissue and lamina propria, and an inner epithelium organized into ridges that run from the base, to the tip of the pouch (Figure 2A). The epithelium is made up of mostly columnar enterocytes and a few mucus secreting goblet cells (Figure 1C). There are four pyloric caeca on the right-hand side of the midgut (Figure 2, "1-4"), two on the left-hand side ("5-6"), and as many as three that are shorter and more proximally restricted ("7-9"). Caeca one through five are present in fish of all four populations (surface, Tinaja, Pachón, and Molino) while six through nine are variable. Surface fish are more likely to have 1-9, Tinaja and Molino 1-6, and Pachón 1-7 (Figure 2C).

The remaining tubular portion of the midgut has inner circumferential and outer longitudinal muscle layers, and the epithelium is folded circumferentially at irregular angles. The epithelium of the proximal midgut is mostly mucus secreting goblet cells that completely lack H&E staining (Figure 1D, D', black arrow), compared to the epithelium of the distal midgut that has goblet cells with basophilic granules (Figure 1E'). The lumen of the distal midgut also contains basophilic enteroendocrine cells that are distinguishable by a smaller size and more apical location (Figure 1E' yellow arrow). A greater number of eosinophilic immune cells are also evident in the lamina propria of the distal region of the midgut (Figure 1E' black arrowhead).

The proximal hindgut is wider than the midgut and has thinner muscle and lamina propria layers (Figure 1F-F'). The enterocytes in the epithelium are highly vacuolated likely representing absorbed hydrophobic molecules (Figure 1F', grey arrow). Apically located enteroendocrine cells are also evident in the epithelium (Figure 1F', yellow arrow). The distal hindgut (rectum) has a thicker muscle wall and connects the GI tract to the anus. Overall, the organization of the *A. mexicanus* gut is similar to other Characiformes. Having established the general anatomy and histology of the GI tract using the surface form, we were next able to explore differences between the surface and cave populations.

Ecotypic differences in gut length

The length of each region of the GI tract is an important variable determining digestive efficiency and can be altered by diet. To determine the ecotypic differences in gut length between populations, we compared relative gut length (gut length divided by fish length) between individually housed fish fed the same diet (38% protein, 7% fat, 5% fiber) and amount per day (6mg). We found that Tinaja (n=6) and Molino (n=5) cavefish tend to have a longer midgut, and Pachón (n=6) cavefish tend to have a shorter midgut compared to surface fish (n=6) (Figure 3A, B). Tinaja and Molino also tend to have a longer hindgut and Pachón have a significantly shorter hindgut compared to surface fish (Figure 2C, p=0.05, one-way ANOVA with Tukey's post hoc test). Interestingly, while all fish were dissected 24 hours post-feeding, we noted a difference in the amount of fecal matter in the gut (Figure 3A). All of the Tinaja cavefish guts were entirely full (n=6), compared to one out of six Pachón, and four out of five Molino. All of the surface fish guts were mostly empty as seen in Figure 3A (n=6). In summary, there are moderate differences in adult gut length between populations that are independent of diet, and some adult cavefish populations may have slower gastrointestinal transit.

Diet influences gut morphology differently in surface fish and Tinaja cavefish

Surface-adapted *A. mexicanus* consume plants and insects throughout the year. In contrast, cavefish populations are subject to seasonal fluctuations, including periods of deprivation. We hypothesized that cavefish may have evolved increased plasticity in gut morphology to maximize nutrient absorption during times of abundance and conserve energy when food is scarce. To test this hypothesis, we switched the diet of adult surface fish and Tinaja cavefish from moderate nutrient content (7% fat, 38% protein, 5% fiber) to either low-nutrient (4% fat, 32% protein, 3% fiber) or high-nutrient (18% fat, 55% protein, 2% fiber). After eight months, we measured the length of the gut segments, as well as the circumference and average number of folds in cross sections, and compared the values to fish that remained on the moderate nutrient diet (Figure 4, n=3 fish per population and diet, and 3 histological sections per segment). On the moderate nutrient diet fed *ad libitum*, Tinaja tend to have a shorter midgut that is wider and has more folds compared to surface

154 fish (relative midgut length: surface = 0.45, Tinaja = .36, circumference: surface = 0.16cm,
155 Tinaja = 0.20, circumference normalized to fish length: surface = 0.03, Tinaja = 0.04, fold
156 number: surface = 6, Tinaja = 9, Figure 4 A-C). Tinaja also tend to have a longer hindgut on
157 this diet as was observed on the controlled diet (surface = 0.17, Tinaja = 0.20).
158 In fish that were switched to a low-nutrient diet, we observed a 24% increase in the
159 length of the midgut in both populations (surface = 0.45 to 0.56, p=0.36; Tinaja = 0.36 to
160 0.44, p = 0.60; one-way ANOVA with HSD post-hoc test, Figure 4A, G). The circumference of
161 the midgut also increased significantly by 89% in surface fish (0.16 to 0.30 cm, normalized
162 to fish length 0.03 to 0.06, p<0.005) and 78% in Tinaja cavefish (0.20 to 0.36 cm,
163 normalized to fish length 0.04 to 0.07, p<0.005, Figure 4B, G). The number of folds in the
164 midgut epithelium increased 2-fold in Tinaja (9 to 18) and nearly 2-fold in surface fish (6 to
165 11). The hindgut length increased by 70% in surface fish (0.17 to 0.28) and only 7% in
166 Tinaja cavefish (0.20 to 0.21, Figure 4D, H). The circumference of the surface fish hindgut
167 did not change significantly (0.34 to 0.33cm, normalized to fish length = 0.06 to 0.07) and
168 the circumference of the Tinaja hindgut increased by 45% in Tinaja (0.24 to 0.35cm,
169 normalized to fish length =0.04 to 0.07, Figure 4D, H). The number of folds in the hindgut
170 epithelium changed only slightly in both populations (Tinaja = 13 to 12, surface = 11 to 13).
171 In summary, midgut length, width, and fold number increased similarly in both populations
172 in response to a low-nutrient diet (Figure 4G). In contrast, the hindgut responds by
173 growing in length in surface fish and, growing in width in cavefish.
174 In fish switched from a moderate to a high-nutrient diet, the length of the midgut did
175 not change in surface fish (0.45 to 0.46, Figure 4A) and decreased in Tinaja cavefish by 20%
176 (0.36 to 0.29). The circumference of the midgut increased in surface fish (0.16 to 0.23cm,
177 normalized to fish length = 0.03 to 0.05) and did not change in cavefish (0.20 to 0.20cm,
178 normalized to fish length = 0.04 to 0.04; Figure 4C). The average number of epithelial folds
179 increased slightly in surface fish (6 to 7) and decreased slightly in the cavefish (9 to 8,
180 Figure 4C). Normalized hindgut length decreased in both populations in response to a high-
181 nutrient diet, although the decrease was greater in Tinaja: 39% (0.20 to 0.12) versus 31%
182 in Surface fish (0.17 to 0.12, Figure 4B). The circumference of the hindgut also decreased,
183 by 26% in surface fish (0.34 to 0.25cm, normalized to fish length = 0.06 to 0.05) and by
184 21% in cavefish (0.24 to 0.19cm) although the value normalized to fish length did not

185 change in cavefish (0.04 to 0.04, Figure 4D). The number of folds in the hindgut decreased
186 by one in surface fish (11 to 10) but more strikingly in Tinaja cavefish reduced to almost
187 half (13 to 7, Figure 4C). In summary, the Tinaja cavefish gut is more responsive than
188 surface fish to a high-nutrient diet since Tinaja cavefish exhibit a greater reduction in
189 midgut and hindgut length and hindgut fold number. Overall, the results suggest that
190 plasticity of the gut is dependent on the type of diet and region of the gut and reveal
191 fundamental differences between the populations.
192
193 *Differences in the regulation of gut proliferation between surface fish and Tinaja cavefish*
194
195 The gastrointestinal epithelium undergoes constant turnover, being replenished by
196 populations of dividing cells that are restricted to the base of villi or epithelial folds (1). We
197 next sought to understand how differences in morphology are achieved by investigating
198 homeostasis of the gut epithelium. We injected fish on the low-nutrient diet with a
199 thymidine analog (5-ethynyl-2'-deoxyuridine, EdU) and, after 24 hours, determined the
200 number of EdU positive cells as a measure of the amount of cell division (Figure 5A, B, F, J).
201 We found that Tinaja cavefish had on average over four times as many EdU positive cells in
202 the midgut (Figure 5F, surface = 103, Tinaja = 449, p = 0.063 two-tailed t-test). Higher
203 proliferation corresponds to a significantly greater number of folds in the midgut
204 epithelium in Tinaja cavefish (Figure 4C, average surface = 11, Tinaja = 18; p = 0.04, two-
205 tailed t-test). However, the number of EdU positive cells per fold in the midgut is also
206 greater in Tinaja (average surface = 11, Tinaja = 26; p = 0.09); EdU positive cells in the
207 epithelium appear more restricted to the base of the folds in surface fish, whereas they
208 extend further up the fold in Tinaja cavefish (Figure 5A, B). In the hindgut, the average
209 number of EdU positive cells is also greater in Tinaja (Figure 5J, surface = 154, Tinaja =
210 354; p = 0.17), although there is only a slight difference in the number of folds (surface =
211 13, Tinaja = 12). These results suggest that altered homeostasis of the gut epithelium could
212 drive morphological differences between the populations.
213 Cavefish evolved in a nutrient-limited environment and unlike surface fish are
214 subject to periods of starvation. Because cell-turnover is energetically expensive, we
215 hypothesized that cavefish may have evolved mechanisms to limit the proliferation in the

gut when food is not available. To test this, we starved fish (for a period of two-weeks) that were previously fed the low-nutrient diet, and compared EdU incorporation over a 24-hour period (Figure 5F, J, K, L). The number of EdU positive cells in the Tinaja midgut decreased significantly by 81% (average 449 fed versus 85 starved, p = 0.005, one-way ANOVA comparing diet and population). In contrast, the number of EdU positive cells nearly doubled in surface fish (average 103 fed versus 193 fasted, p = 0.63). In both populations, midgut length, circumference, and fold number decreased in response to starvation (Figure 5C-D). In surface fish, the midgut length shortened significantly by 40% (0.56 to 0.34, p=0.01, one-way ANOVA) compared to only 19% in Tinaja cavefish (0.44 to 0.36, p=0.42). The midgut circumference decreased by 25% in surface fish (0.30 to 0.23cm, normalized to fish length = 0.06 to 0.05) and significantly in cavefish by 34% (0.36 to 0.24cm, p=0.004, normalized to fish length = 0.07 to 0.05; p=0.03). The number of folds in the midgut decreased from 11 to 7 in surface fish (p=0.53) and more dramatically, from 18 to 6 in Tinaja cavefish (p=0.01). In summary, Tinaja cavefish reduce proliferation in response to starvation and this is associated with a substantial decrease in midgut circumference and fold number, but a more moderate decrease in length, compared to surface fish.

In the hindgut, the average number of EdU positive cells also reduced significantly in Tinaja cavefish in response to starvation (Figure 5J, average 354 to 130, p=0.005, one-way ANOVA), and to a lesser extent in surface fish (38%, average 154 to 95, p= 0.63 one-way ANOVA). Relative hindgut length reduced by 50% in surface fish (0.28 to 0.14) and only 20% in Tinaja (0.21 to 0.15). We observed a similar reduction in hindgut circumference, by 35% in surface fish (0.33 to 0.21cm, normalized to fish length = 0.07 to 0.04) and 34% in Tinaja cavefish (0.35 to 0.23cm, normalized to fish length = 0.07 to 0.05). The number of hindgut folds reduced from 13 to 8 in surface fish and 12 to 6 in Tinaja cavefish. Similar to what occurs in the midgut, in the hindgut, Tinaja decrease proliferation more substantially in response to starvation but have a less drastic decrease in length compared to surface fish. Combined, our findings support the hypothesis that cavefish have mechanisms for tuning gut homeostasis in response to food intake that differ from surface fish.

Genetic mapping reveals quantitative trait loci associated with hindgut length

247 We next sought to understand the genetic basis of differences in gut morphology
248 between surface fish and cavefish. We carried out a quantitative trait loci (QTL) analysis
249 using F2 surface/Tinaja hybrids (see methods). To eliminate the effect of diet or appetite,
250 we individually housed the hybrids as adults and ensured they consumed the same diet
251 (38% protein, 7% fat, 5% fiber) and amount per day (6mg). After four months, we
252 determined the length and weight of the fish, number of pyloric caeca, and length of the
253 midgut and hindgut. We identified a QTL for female body condition (fish weight/fish
254 length) on linkage group 13 with a LOD score of 5.53 accounting for 21% of the variance in
255 this trait (Figure 6B). We did not identify a QTL for male body condition (fish weight/fish
256 length Figure 6A). We also did not identify a significant QTL for pyloric caeca number but
257 observed a peak on linkage group 24 (Figure 6C).
258 There is a strong positive correlation between fish length and gut length as
259 anticipated (midgut p-value=2.2x10^-16, hindgut p-value=5.2x10^-14, Pearson's product-
260 moment correlation). We therefore performed the QTL analysis using relative gut length.
261 We did not identify a significant QTL for relative midgut length but observed a peak on
262 linkage group 14 (Figure 6D). We found a significant QTL for relative hindgut length on
263 linkage group 10 with a LOD score of 4.82 at the peak marker r172341 accounting for 11%
264 of the variance in this trait. Interestingly, it is the heterozygous genotype at this position
265 that is associated with longest relative hindgut length (Figure 7C). Similarly, F1 hybrids
266 have a longer hindgut than surface fish or Tinaja cavefish (Figure 7A,B). The midgut of F1
267 hybrids is also longer; however, when we examined the effect plot for the marker with the
268 highest LOD score for relative midgut length, we found that individuals with cave genotype
269 have the longest midgut (Figure 7D, E). Combined, the results indicate overdominance or
270 positive epistasis in the genetic network controlling gut length.
271
272 *Candidate genes controlling hindgut length*
273
274 To search for genetic changes that contribute to variation in hindgut length, we used
275 a combination of population genetics and differential gene expression analysis. We first
276 used the Pachón cavefish genome assembly to identify the position of markers that define
277 the 1.5-LOD support interval for the hindgut QTL. We found that two markers are on

278 scaffold KB882083 and one is on KB871783 (Table 1). We determined several population
279 genetic metrics for all of the genes on each scaffold using whole genome sequencing data
280 (Dataset S1, 18). This data set includes Tinaja, Pachón and Molino cave populations and
281 two surface populations: Río Choy, which is representative of our lab strains and is more
282 closely related to the stock of fish that invaded the Molino cave, and Rascón, which is more
283 representative of a separate stock of surface fish that invaded the Tinaja and Pachón caves.
284 We found that 45 genes within the 1.5-LOD support interval for the hindgut QTL have fixed
285 differences in the coding regions between Río Choy surface fish (n=9) and Tinaja cavefish
286 (n=10) populations (Dataset S1, all on scaffold KB882083). Ten of these genes may be
287 under selection since the haplotype including the genes exhibits evidence of non-neutral
288 evolution comparing Río Choy to Tinaja (Max pairwise divergence = 1 and significant
289 HapFLK p-values (< 0.05), Table 2, Figure 8A). Two of the ten genes also fit within the same
290 statistical parameters comparing Rascón surface fish to Tinaja cavefish (Table 2). These
291 two genes are predicted to encode complement factor B-like proteins that are involved in
292 innate immunity (herein referred to as Cfb1 and Cfb2). We found that *cfb1/2* also have
293 significant HapFLK p-values comparing Pachón to surface populations, but not to Molino
294 (Table 2). The ten genes with significant HapFLK values in Tinaja have varying ranks of
295 divergence in the other cave populations (Figure 8A,B). Genes that show high levels of
296 divergence in all populations may be generally important for cave adaptation (e.g. *cfb1/2*,
297 Figure 8A, B). Genes that show divergence in only the Tinaja population (e.g. *klf5l*) may be
298 important for adaptation only in the Tinaja cave.
299 Next, we explored which genes in the QTL may have regulatory mutations by
300 comparing levels of expression. For this analysis, we utilized the surface fish genome
301 assembly that is organized into chromosomes. We found that the markers that define the
302 estimated confidence interval for the hindgut QTL are on chromosome 14 and span a
303 region of approximately 15KB (Table 1). This region has 342 genes. We determined if any
304 of these genes are differentially expressed in the hindgut using RNA sequencing data from
305 adult surface, Tinaja, and surface/Tinaja F1 hindguts (30) (n=5 hindguts per population).
306 We found that 31 genes are differentially expressed using a likelihood ratio test to compare
307 all three sample types (Table S1). Pairwise comparison between Tinaja cavefish and
308 surface fish revealed 9 additional differentially expressed genes (Table S1). Included in this

309 list is *cfb1*. Tinaja cavefish exhibit the highest expression of *cfb1* and expression in the F1
310 hybrid is intermediate (Figure 8C). We reasoned that genes showing either the greatest or
311 lowest expression in F1 hybrids may be strong candidates for controlling differences in
312 length since the heterozygous genotype at the QTL is associated with the longest hindgut.
313 Of the genes that are in the QTL and differentially expressed, five show the highest
314 expression in the hybrid and eight show the lowest expression in the hybrid. Among the
315 genes that are lowest in the hybrid is *Notch1A* (Figure 8C, Table S1). Notch signaling
316 controls stem cell renewal and formation of secretory versus absorptive cell fate in the
317 intestine (31).
318
319 *Expression patterns associated with differences in gut length*
320
321 We next broadened our analysis of the RNA sequencing data to investigate other
322 pathways that may have been altered during the evolution of the cavefish gut; 3550 genes
323 are differentially expressed between surface, F1 hybrids, and Tinaja hindguts (30). We
324 searched for patterns across the differentially expressed genes between sample groups
325 (degPatterns function in DEseq 2, Figure S1) and identified clusters of genes that show
326 either greatest (Table S2, group 3, n=55) or lowest (Table S3, group4, n=53) expression in
327 the F1 hybrid, reasoning that these may be more likely to be associated with differences in
328 hindgut length. The genes that have the greatest expression in the hybrid include an
329 additional component of the complement system (*C8G*), a negative regulator of Notch
330 signaling (*nrarpa*), retinoic acid signaling components (*Cyp26A1, rdh1*), and a circadian
331 rhythm gene (*timeless*) (Figure 8C). The genes that show a pattern of lowest expression in
332 the hybrid include tumor suppressor and apoptosis related genes (*casp6, brca2, pak1*), a
333 suppressor of cytokine activity (not annotated), regulator of retinoic acid production
334 (*bco1*), and a circadian rhythm gene that typically correlates with timeless expression
335 (*per1b*) (Figure 8C). In summary, we found that surface fish and cavefish have differences
336 in the genetic architecture controlling hindgut length, and that cavefish have altered
337 expression of genes controlling cell proliferation, cell signaling, and immune system
338 function.
339

Discussion

A major challenge for *Astyanax mexicanus* when they invaded caves was adapting to the drastically limited availability of nutrients compared to what they experienced in the ancestral river environment. In response, they evolved hyperphagia, starvation resistance, and increased fat accumulation (27, 28, 32). Here, we investigated how the morphology and homeostasis of their gastrointestinal tract adapted as a consequence of nutrient restriction. Our data suggest that specializations for individual caves may have occurred. By comparing fish on the same diet in the laboratory, we found that Tinaja and Molino cave populations converged on a lengthened gut while Pachón have a shortened gut. A plausible explanation for this is differences in cave ecology; the Pachón cave is less impacted by seasonal flooding and has cave-adapted micro-crustaceans that serve as a food source for post-larval fish (16). In all cave populations, we observed a reduction in the number of pyloric caeca, specifically absence of caeca 7-9. The pyloric caeca may have roles in digestion, absorption, and immune system function (33, 34). It is possible that caeca 7-9 are important for digestion of foods, or response to pathogens, that are only present in the surface fish environment, and these structures became vestigial and eventually disappeared in the cave. Other groups of fish like salmonids can have hundreds of pyloric caeca (35). Our study establishes a genetically accessible model to understand pyloric caeca function, development, and evolution.

We hypothesized that cavefish evolved increased plasticity of the gut as an adaptation to save energy during seasonal fluctuation of food. The most striking difference that we observed between populations is that cavefish have much greater proliferation in the gut epithelium compared to surface fish under fed conditions and reduce proliferation in response to food deprivation. Cavefish may have increased sensitivity in the pathways that sense or respond to nutrient shortage and it is plausible that this provides an advantage in the cave. On a high-nutrient diet, cavefish exhibit a more dramatic reduction in gut length compared to surface fish. Reducing length when nutrients are abundant could achieve a more optimal balance between energy extraction and storage; the gut is packaged within the body cavity and its size could limit the amount of visceral fat that can accumulate. How the cellular dynamics of the epithelium translate to changes in gut

371 morphology are not entirely clear. For example, proliferation increases in surface fish
372 during starvation, yet gut length decreases. The balance between cell renewal and death is
373 likely different between the populations and in line with this, we observed that Tinaja have
374 lower expression of tumor-suppressor and pro-apoptosis genes (i.e. *brca2*, *p21-activated*
375 *kinase*, *caspase 6*). Overall, while we observe plasticity in gut morphology in both surface
376 fish and cavefish, our data support the hypothesis that cavefish have a more dramatic
377 response to nutrient fluctuations.

378 At post-larval stages, Pachón cavefish have altered gastrointestinal motility,
379 resulting in delayed transit of ingested food (29). Here we found evidence of slower transit
380 of digestive material in adult cavefish populations as well. Tinaja, Pachón, and Molino guts
381 were full 24-hours after feeding, compared to surface fish guts that were mostly empty.
382 Slower transit time may have evolved to optimize digestion of decaying material mixed
383 with mud, a likely way food is obtained in the caves, and/or could result in increased
384 nutrient absorption. Our results highlight that altered gut function and morphology likely
385 accompany adaptation to the food sources in the cave.

386 We found evidence that the genetic architecture controlling gut morphology
387 diverged between surface fish and Tinaja cavefish. We identified a QTL associated with
388 hindgut length and found that F1 and heterozygous F2 hybrids have a longer hindgut
389 compared to surface fish and cavefish. This phenomenon (heterosis) has been observed for
390 another *A. mexicanus* trait, thickness of the inner retina (36), and is often seen in plant
391 breeding, yet the genetic and molecular basis is not easy to define (37). One hypothesis is
392 that each parent has genetic changes that result in an inferior phenotype, and that in the
393 hybrid these changes are complemented, resulting in a superior phenotype (Dominance).
394 Another possibility is that there are multiple alleles that interact in a way that produces a
395 phenotype greater than what could be achieved in a homozygous condition (Over-
396 dominance). It is possible that there are multiple alleles that have antagonistic effects on
397 hindgut length and when they are combined the result is a longer gut.

398 To investigate which genes in the QTL may be important for controlling gut length
399 we used a combination of population genetics and RNA sequencing. Our results revealed
400 two genes that are known to regulate intestinal homeostasis in other species, *klf5* (krüppel-
401 like factor 5) and *Notch1A*. KLF5 is a transcription factor expressed in intestinal crypts that

402 can promote or inhibit proliferation and is commonly dysregulated in colon cancer (38–
403 40). Notch signaling balances stem cell renewal and differentiation; activation of Notch
404 signaling promotes stem cell proliferation and suppresses secretory cell formation (31).
405 We found evidence that *klf5l* may be under selection in the Tinaja cave as we observed
406 significant HapFLK p-values comparing Tinaja to Rio Choy surface fish. While we did not
407 find the same evidence for the *notch1a* coding region, we found that expression of *notch1a*
408 is significantly different between surface fish, Tinaja cavefish, and F1 hybrids, suggesting
409 there may be regulatory mutations within the QTL that influence *notch1a* expression.
410 Tinaja cavefish tend to have higher n*otch1a* expression, in line with greater proliferation in
411 the epithelium. However, we found that notch-regulated ankyrin repeat protein (*nrarpa*)
412 that suppresses Notch signaling in other contexts (41, 42) is more highly expressed in both
413 Tinaja cavefish and F1 hybrids. Since Notch signaling tends to be context dependent,
414 comparing the components of the Notch signaling pathway with cellular resolution may
415 give insight into how differences in proliferation and morphology arise.
416 Cave-adapted *A. mexicanus* not only experience a different diet in the cave, but also a
417 different microbial landscape (43). We found that complement factor B (*cfb1*) is within the
418 hindgut QTL, shows significant divergence in all populations, and is differentially expressed
419 in the hindgut. Complement factor B is part of the innate immune system. It is expressed in
420 multiple tissues, including the colonic mucosa, and functions in the pathway that
421 recognizes and eliminates bacterial pathogens by controlling immune cell differentiation
422 (44, 45). Mounting evidences suggests that immune cells alter self-renewal of stem cells in
423 the epithelium through cytokine signaling (5). Interestingly, we found that cavefish and F1
424 hybrids have lower expression of a suppressor of cytokine signaling in the hindgut. Recent
425 research suggests that Pachón cavefish have fewer pro-inflammatory immune cells in the
426 visceral adipose tissue (46), but the amount and differences in the immune cells in the gut
427 have not been explored. Our results suggest that evolution of the immune system in *A.*
428 *mexicanus* likely plays a role in how the gut responds to external cues. In the lab, the
429 external microbial landscape is the same for the populations, yet it is possible that genetic
430 differences select for specific microbes and this in turn influences intestinal homeostasis.
431 Cavefish accumulate more carotenoids (retinoic acid (RA) precursors) in the
432 visceral adipose tissue compared to surface fish and this correlates with decreased

433 expression of genes that convert carotenoids into retinoids in the gut epithelium (47). We
434 found that cavefish and F1 hybrids have lower expression of beta-carotene oxygenase
435 (*bco1*) and higher expression of retinol dehydrogenase (*rhd1*) in the hindgut. The outcome
436 may be changes in RA production and signaling. RA signaling is important for stem cell
437 maintenance in a number of contexts (48), but how it regulates intestinal stem cell
438 homeostasis *in vivo* is not well understood. However, it is clear that RA signaling regulates
439 innate immune cells in the gut (49). It is possible that altered RA signaling in the cavefish
440 gut influences the crosstalk between immune cells and stem cells resulting in differences in
441 morphology.
442 We found that expression of the circadian clock genes *per1* and *timeless*, which are
443 typically synchronized, show the opposite expression pattern in the hindguts of cavefish
444 and F1 hybrids. Proliferation and gene expression in the intestine is under circadian
445 control and disruption of clock genes alters renewal of the epithelium (50–52). Having
446 evolved in complete darkness, cavefish have altered circadian rhythm as evidenced by
447 developmentally delayed and reduced amplitude of clock gene expression, lack of circadian
448 cycles of metabolism, and reduced sleep (26, 53–55). It is plausible that alterations to the
449 gene regulatory network controlling circadian rhythm influenced homeostasis of the
450 intestinal epithelium during cavefish evolution. Overall, our study reveals multiple levels at
451 which the *A. mexicanus* gut has evolved in response to ecological differences in food
452 availability including morphology, homeostasis, and plasticity in response to dietary
453 fluctuations. Furthermore, we implicate genetic changes and molecular pathways that may
454 have accompanied evolution of these traits.
455
456 **Methods**
457 *Fish husbandry and diet*
458 Fish husbandry was performed according to (56). For fixed diet experiments fish were
459 housed individually in 1.5L tanks and fed three pellets (approximately 6mg) of New Life
460 Spectrum TheraA+ small fish formula once per day for at least 4 months. Commercially-
461 available low nutrient (Hikari Goldfish Staple), moderate nutrient (New Life Spectrum
462 TheraA+), and high-nutrient (Ken's Premium Growth Meal #3) diets were fed *ad libitum.*
463

464 *Phenotype quantification and data visualization*

465 Fish were euthanized in 1400ppm Tricane and dissected 24-hours post feeding. Images
466 were taken using a Cannon Powershot D12 digital camera. ImageJ was used to measure fish
467 length and gut length. Data visualization was performed using R (57).

468

469 *Histology and imaging*

470 Figure 1: The fish was euthanized in 1400 ppm tricane, an incision was made along the
471 ventral body line, and it was placed into 10% buffered formalin and shipped to FishVet
472 Group (Portland, ME) for further processing. The gut was dehydrated using a graded
473 ethanol series, followed by several changes in xylene, and then embedded in paraffin.
474 Sections were taken at 5μm thickness, stained with hematoxylin and eosin (H&E) and
475 imaged using Aperio ScanScope CS. Figure 4,5: To quantify proliferation, fish were
476 anesthetized using 400ppm Tricane, then 40μL of EdU (500μM in .1% DMSO) was injected
477 into the intraperitoneal cavity using an insulin syringe. After 24 hours, fish were
478 euthanized in 1400 ppm tricane and the gut was immediately removed, incubated
479 overnight in 10% formalin, then washed in PBS and dehydrated to 100% ethanol through a
480 graded ethanol series. The gut was incubated briefly in Histo-clear (National Diagnostics).
481 The midgut and hindgut were separated and embedded in paraffin side by side in a single
482 block in anterior to posterior orientation to obtain a transverse section of each structure.
483 Blocks were sectioned at a thickness of 5μm using a Leica RM 2155 rotary microtome.
484 Slides were dried overnight, deparaffinized using Histo-clear, and rehydrated to water
485 through a graded ethanol series. The slides were placed in 10% buffered formalin for 10
486 minutes and washed twice in 3% Bovine Serum Albumin (BSA). EdU was detected using
487 the Click-IT EdU Cell Proliferation Kit (ThermoFisher) according to the manufacturers
488 protocol. Slides were mounted in ProLong Gold (ThermoFisher) and images were taken
489 using Keyence BZ2 microscope and software. We measured tissue morphology and EdU
490 cell number manually using ImageJ (58).

491

492 ***Quantitative trait loci analysis***

493 *F2 hybrid population.* We bred a surface fish female with a Tinaja cavefish male to produce
494 a clutch of F1 hybrids. We generated a population of surface/Tinaja F2 hybrids by
495 interbreeding individuals from this clutch. The F2 mapping population (n=219) consisted
496 of three clutches produced from breeding paired F1 surface/Tinaja hybrid siblings.
497
498 *Genotype by sequencing.* We extracted DNA from caudal tail fins using DNeasy Blood and
499 Tissue DNA extraction kit (Qiagen). DNA was shipped to Novogene (Chula Vista, CA) for
500 quality control analysis and sequencing. Samples that contained greater than 1.5 ug DNA,
501 minimal degradation (as determined by gel electrophoresis), and OD_{260}/OD_{280} ratio of 1.8
502 to 2.0 were used for library construction. Each genomic DNA sample (0.3~0.6 μg) was
503 digested with Mse1, HaeIII, and EcoR1. Digested fragments were ligated with two barcoded
504 adapters: a compatible sticky end with the primary digestion enzyme and the Illumina P5
505 or P7 universal sequence. All samples were pooled and size-selected after several rounds of
506 PCR amplification to obtain the required fragments needed to generate DNA libraries.
507 Concentration and insert size of each library was determined using Qubit® 2.0 fluorometer
508 and Agilent® 2100 bioanalyzer respectively. Finally, quantitative real-time PCR (qPCR) was
509 used to detect the effective concentration of each library. Qualified DNA libraries had an
510 effective concentration of greater than 2 nM and were pooled by effective concentration
511 and expected data production. Pair-end sequencing was then performed on Illumina®
512 HiSeq platform, with the read length of 144 bp at each end. Raw Illumina genotype-by-
513 sequencing reads were cleaned and processed through the *process_shortreads* command in
514 the Stacks software package (59). The cleaned reads were aligned to the *Astyanax*
515 *mexicanus* reference genome (AstMex102, INSDC Assembly GCA_000372685.1, Apr 2013)
516 using the Bowtie2 software (60). The aligned reads of 4 surface fish, 4 Tinaja cavefish and 4
517 F_1 surface/Tinaja hybrids were manually stacked using the *pstacks* command. We then
518 assigned the morphotypic origin of each allele and confirmed heterozygosity in the F_1
519 samples using the *cstacks* command. Finally, we used this catalog to determine the
520 genotypes at each locus in the F2 samples with the *sstacks* and *genotypes* command. This
521 genotype database was formatted for use in R/qtl (61)
522

523 *Linkage map.* Using R/qtl, we selected for markers that were homozygous and had opposite
524 genotypes in cavefish versus surface fish (based on three surface and three cave
525 individuals). A linkage map was constructed from these loci using only the F2 population.
526 All markers that were genotyped in less than 180 individuals were omitted, as well as all
527 individuals that had poor marker genotyping (<1500 markers). Markers that did not
528 conform to the expected allele segregation ratio of 1:2:1 were also omitted ($p < 1e^{-10}$).
529 These methods produced a map with 1839 markers, 219 individuals, and 29 linkage
530 groups. Unlinked markers and small linkage groups (<10 markers) were omitted until our
531 map consisted of the optimal 25 linkage groups (*Astyanax mexicanus* has 2n = 50
532 chromosomes (62)). Each linkage group had 20-135 markers and markers were reordered
533 by default within the linkage groups, producing a total map length of > 5000 cM. Large gaps
534 in the map were eliminated by manually switching marker order to the best possible order
535 within each linkage group (error.prob = 0.005). The final linkage map consisted of 1800
536 markers, 219 individuals and 25 linkage groups, spanning 2871 cM. Maximum spacing was
537 32.1 cM and average spacing was 1.6 cM.
538
539 *QTL scan using R/qtl.* Genome wide logarithm of the odds (LOD) scores were calculated
540 using a single-QTL normal model and Haley-Knott regression. We assessed statistical
541 significance of LOD scores by calculating the 95th percentile of genome-wide maximum
542 penalized LOD score using 1000 random permutations (scanone). We estimated the
543 confidence intervals for identified QTL as the 1.5-LOD support interval expanded to the
544 nearest genotyped marker (lodint).
545
546 ***Population genomic metrics and analysis***
547
548 We performed the following measures with GATK-processed data, including a core
549 set of samples analyzed in previous studies (18, 28) which contained: Pachón, N = 10 (9
550 newly re-sequenced plus the reference reads mapped back to the reference genome);
551 Tinaja N =10; Molino N = 9; Rascón N = 8; and Río Choy N = 9 and required six or more
552 individuals have data for a particular site. Details of sequencing and sample processing are
553 in (18, 28). We used VCFtools v0.1.13 (63) to calculate π, F_{ST} and d_{XY} and custom python

554 scripts to calculate these metrics on a per gene basis. We identified the allele counts per
555 population with VCFtools and used these for subsequent d_{XY} and fixed differences (D_F)
556 calculations. We used hapFLK v1.3 https://forge-dga.jouy.inra.fr/projects/hapflk (64) for
557 genome-wide estimation of the hapFLK statistic of across all 44 *Astyanax mexicanus*
558 samples and two *Astyanax aeneus* samples. For all of these metrics, we only used sites that
559 contained six or more individuals per population and calculated the metric or included the
560 p-values (in the case of hapFLK) for only the coding region of the gene. Candidate genes
561 were included if (a) the comparison between Río Choy and Tinaja resulted in a maximum
562 $d_{XY} = 1$, suggesting that there was at least one fixed difference between Río Choy and Tinaja
563 and (b) HapFLK resulted in at least one p value less than 0.05, suggesting that the
564 haplotype surrounding the gene exhibited evidence for non-neutral evolution.
565
566 ***RNA sequencing***
567 *RNA extraction and cDNA synthesis.* Adult *A. mexicanus* were euthanized in 1400ppm
568 Tricane and the hindgut was immediately removed and homogenized in 0.3mL Trizol using
569 a motorized pellet pestle, and then stored at -80°C. Total RNA was extracted using Zymo
570 Research Direct-zol RNA MicroPrep with DNAse treatment according to the manufacturers
571 protocol. LunaScript RT supermix kit with 1μg of RNA was used to synthesize cDNA. All
572 samples were processed on the same day. Diluted cDNA samples (50ng/μL) were used for
573 sequencing.
574
575 *RNA sequencing and differential gene expression analysis.* HiSeq Illumina sequencing was
576 performed by Novogene (Chula Vista, CA). All samples were indexed and run as pools,
577 providing an estimated 20-30 million single-end reads per sample. Samples were
578 processed using an RNA-seq pipeline implemented in the bcbio-nextgen project
579 (https://bcbio-nextgen.readthedocs.org/en/latest/). Raw reads were examined for quality
580 issues using FastQC (http://www.bioinformatics.babraham.ac.uk/projects/fastqc/) to
581 ensure library generation and sequencing are suitable for further analysis.
582 Reads were aligned to Ensembl build 2 of the *Astyanax mexicanus* genome, augmented with
583 transcript information from Ensembl release 2.0.97 using STAR (65) with soft trimming

584 enabled to remove adapter sequences, other contaminant sequences such as polyA tails
585 and low quality sequences. Alignments were checked for evenness of coverage, rRNA
586 content, genomic context of alignments and complexity using a combination of FastQC,
587 Qualimap (66), MultiQC (https://github.com/ewels/MultiQC), and custom tools. Counts of
588 reads aligning to known genes were generated by featureCounts (67) and used for further
589 QC with the R package bcbioRNASeq [Steinbaugh MJ, Pantano L, Kirchner RD et al.
590 bcbioRNASeq: R package for bcbio RNA-seq analysis [version 2; peer review: 1 approved, 1
591 approved with reservations]. F1000Research 2018, 6:1976
592 (https://doi.org/10.12688/f1000research.12093.2)]. In parallel, Transcripts Per Million
593 (TPM) measurements per isoform were generated by quasialignment using Salmon (68)
594 for downstream differential expression analysis as quantitating at the isoform level has
595 been shown to produce more accurate results at the gene level (69). Salmon output was
596 imported into R using tximport (70) and differential gene expression analysis and data
597 visualization was performed using R with the DEseq 2 package (57, 71).
598

599 **Acknowledgments**

600 Brian Martineu and Megan Peavey for fish husbandry. This work was supported by grants
601 from the National Institutes of Health [HD089934, DK108495].
602

603 **References**

604 1. H. Gehart, H. Clevers, Tales from the crypt: new insights into intestinal stem cells.
605 *Nat. Rev. Gastroenterol. Hepatol.* **16**, 19–34 (2019).
606 2. S. Beyaz, *et al.*, High-fat diet enhances stemness and tumorigenicity of intestinal
607 progenitors. *Nature* **531**, 53–58 (2016).
608 3. C.-W. Cheng, *et al.*, Ketone Body Signaling Mediates Intestinal Stem Cell Homeostasis
609 and Adaptation to Diet. *Cell* **178**, 1115-1131.e15 (2019).
610 4. C. A. Lindemans, *et al.*, Interleukin-22 promotes intestinal-stem-cell-mediated
611 epithelial regeneration. *Nature* **528**, 560–564 (2015).
612 5. M. Biton, *et al.*, T Helper Cell Cytokines Modulate Intestinal Stem Cell Renewal and
613 Differentiation. *Cell* **175**, 1307-1320.e22 (2018).
614 6. D. M. Smith, R. C. Grasty, N. A. Theodosiou, C. J. Tabin, N. M. Nascone-Yoder,

615 Evolutionary relationships between the amphibian, avian, and mammalian stomachs.
616 *Evol. Dev.* **2**, 348–359 (2000).
617 7. K. D. Walton, D. Mishkind, M. R. Riddle, C. J. Tabin, D. L. Gumucio, Blueprint for an
618 intestinal villus: Species-specific assembly required. *Wiley Interdiscip. Rev. Dev. Biol.*
619 **7**, e317 (2018).
620 8. N. A. Theodosiou, E. Oppong, 3D morphological analysis of spiral intestine
621 morphogenesis in the little skate, <scp> *Leucoraja erinacea* </scp>. *Dev. Dyn.* **248**,
622 688–701 (2019).
623 9. S. Takashima, D. Gold, V. Hartenstein, Stem cells and lineages of the intestine: a
624 developmental and evolutionary perspective. *Dev. Genes Evol.* **223**, 85–102 (2013).
625 10. I. Miguel-Aliaga, H. Jasper, B. Lemaitre, Anatomy and Physiology of the Digestive
626 Tract of Drosophila melanogaster. *Genetics* **210**, 357–396 (2018).
627 11. N. Aghaallaei, *et al.*, Identification, visualization and clonal analysis of intestinal stem
628 cells in fish. *Development* **143**, 3470–3480 (2016).
629 12. S. C. Leigh, B.-Q. Nguyen-Phuc, D. P. German, The effects of protein and fiber content
630 on gut structure and function in zebrafish (Danio rerio). *J. Comp. Physiol. B* **188**, 237–
631 253 (2018).
632 13. S. M. Secor, Digestive physiology of the Burmese python: broad regulation of
633 integrated performance. *J. Exp. Biol.* **211**, 3767–3774 (2008).
634 14. S. R. McWilliams, W. H. Karasov, Phenotypic flexibility in digestive system structure
635 and function in migratory birds and its ecological significance. *Comp. Biochem.*
636 *Physiol. Part A Mol. Integr. Physiol.* **128**, 577–591 (2001).
637 15. A. L. Andrew, *et al.*, Growth and stress response mechanisms underlying post-feeding
638 regenerative organ growth in the Burmese python. *BMC Genomics* **18**, 338 (2017).
639 16. L. Espinasa, *et al.*, Contrasting feeding habits of post-larval and adult Astyanax
640 cavefish. *Subterr. Biol.* **21**, 1–17 (2017).
641 17. G. Spicher, [Cytochrome absorption spectra of bacteria as aid for solving taxonomic
642 problems. 1. Elaboration and description of a method for measuring the redox and
643 carbon monoxide difference spectra of suspensions of intact live bacterial cells
644 (author's transl)]. *Zentralbl. Bakteriol. Orig. A.* **226**, 524–40 (1974).
645 18. A. Herman, *et al.*, The role of gene flow in rapid and repeated evolution of cave-

646 related traits in Mexican tetra, Astyanax mexicanus. *Mol. Ecol.* **27**, 4397–4416 (2018).
647 19. M. E. Protas, *et al.*, Genetic analysis of cavefish reveals molecular convergence in the
648 evolution of albinism. *Nat. Genet.* **38**, 107–111 (2006).
649 20. S. E. McGaugh, *et al.*, The cavefish genome reveals candidate genes for eye loss. *Nat.*
650 *Commun.* **5** (2014).
651 21. A. K. Powers, E. M. Davis, S. A. Kaplan, J. B. Gross, Cranial asymmetry arises later in
652 the life history of the blind Mexican cavefish, Astyanax mexicanus. *PLoS One* **12**
653 (2017).
654 22. H. Hinaux, *et al.*, Sensory evolution in blind cavefish is driven by early embryonic
655 events during gastrulation and neurulation. *Development* **143**, 4521–4532 (2016).
656 23. J. E. Kowalko, *et al.*, Loss of schooling behavior in cavefish through sight-dependent
657 and sight-independent mechanisms. *Curr. Biol.* **23**, 1874–1883 (2013).
658 24. M. Yoshizawa, *et al.*, Distinct genetic architecture underlies the emergence of sleep
659 loss and prey-seeking behavior in the Mexican cavefish. *BMC Biol.* **13**, 15 (2015).
660 25. J. Jaggard, *et al.*, The lateral line confers evolutionarily derived sleep loss in the
661 Mexican cavefish. *J. Exp. Biol.* **220**, 284–293 (2017).
662 26. D. Moran, R. Softley, E. J. Warrant, Eyeless Mexican cavefish save energy by
663 eliminating the circadian rhythm in metabolism. *PLoS One* **9**, e107877 (2014).
664 27. A. C. Aspiras, N. Rohner, B. Martineau, R. L. Borowsky, C. J. Tabin, Melanocortin 4
665 receptor mutations contribute to the adaptation of cavefish to nutrient-poor
666 conditions. *Proc. Natl. Acad. Sci.* **112**, 9668–9673 (2015).
667 28. M. R. Riddle, *et al.*, Insulin resistance in cavefish as an adaptation to a nutrient-
668 limited environment. *Nature* **555**, 647–651 (2018).
669 29. M. R. Riddle, W. Boesmans, O. Caballero, Y. Kazwiny, C. J. Tabin, Morphogenesis and
670 motility of the Astyanax mexicanus gastrointestinal tract. *Dev. Biol.* **441**, 285–296
671 (2018).
672 30. M. R. Riddle, *et al.*, Genetic architecture underlying changes in carotenoid
673 accumulation during the evolution of the Blind Mexican cavefish,
674 Astyanax mexicanus *bioRxiv*, 788844 (2019).
675 31. E. S. Demitrack, L. C. Samuelson, Notch regulation of gastrointestinal stem cells. *J.*
676 *Physiol.* **594**, 4791–4803 (2016).

677 32. S. Xiong, J. Krishnan, R. Peuß, N. Rohner, Early adipogenesis contributes to excess fat
678 accumulation in cave populations of Astyanax mexicanus. *Dev. Biol.* **441**, 297–304
679 (2018).
680 33. R. K. Buddington, J. M. Diamond, Aristotle revisited: the function of pyloric caeca in
681 fish. *Proc. Natl. Acad. Sci.* **83**, 8012–8014 (1986).
682 34. N. A. Ballesteros, *et al.*, The Pyloric Caeca Area Is a Major Site for IgM+ and IgT+ B Cell
683 Recruitment in Response to Oral Vaccination in Rainbow Trout. *PLoS One* **8**, e66118
684 (2013).
685 35. L. D. Townsend, Variation in the Number of Pyloric Caeca and Other Numerical
686 Characters in Chinook Salmon and in Trout. *Copeia* **1944**, 52 (1944).
687 36. K. E. O'Quin, M. Yoshizawa, P. Doshi, W. R. Jeffery, Quantitative Genetic Analysis of
688 Retinal Degeneration in the Blind Cavefish Astyanax mexicanus. *PLoS One* **8**, e57281
689 (2013).
690 37. J. A. Birchler, H. Yao, S. Chudalayandi, Unraveling the genetic basis of hybrid vigor.
691 *Proc. Natl. Acad. Sci.* **103**, 12957–12958 (2006).
692 38. B. B. McConnell, *et al.*, Krüppel-Like Factor 5 Is Important for Maintenance of Crypt
693 Architecture and Barrier Function in Mouse Intestine. *Gastroenterology* **141**, 1302-
694 1313.e6 (2011).
695 39. T. Nakaya, *et al.*, KLF5 Regulates the Integrity and Oncogenicity of Intestinal Stem
696 Cells. *Cancer Res.* **74**, 2882–2891 (2014).
697 40. X. Zhang, *et al.*, Somatic Superenhancer Duplications and Hotspot Mutations Lead to
698 Oncogenic Activation of the KLF5 Transcription Factor. *Cancer Discov.* **8**, 108–125
699 (2018).
700 41. T. Ishitani, K. Matsumoto, A. B. Chitnis, M. Itoh, Nrarp functions to modulate neural-
701 crest-cell differentiation by regulating LEF1 protein stability. *Nat. Cell Biol.* **7**, 1106–
702 1112 (2005).
703 42. T. J. Yun, M. J. Bevan, Notch-Regulated Ankyrin-Repeat Protein Inhibits Notch1
704 Signaling: Multiple Notch1 Signaling Pathways Involved In T Cell Development. *J.*
705 *Immunol.* **170**, 5834–5841 (2003).
706 43. P. Ornelas-García, S. Pajares, V. M. Sosa-Jiménez, S. Rétaux, R. A. Miranda-Gamboa,
707 Microbiome differences between river-dwelling and cave-adapted populations of the

708 fish Astyanax mexicanus (De Filippi, 1853). *PeerJ* **6**, e5906 (2018).
709 44. J. Laskowski, J. M. Thurman, "Chapter 14 - Factor B" in *The Complement FactsBook*
710 *(Second Edition)*, Factsbook., Second Edi, S. Barnum, T. Schein, Eds. (Academic Press,
711 2018), pp. 135–146.
712 45. Andoh, *et al.*, Detection of complement C3 and factor B gene expression in normal
713 colorectal mucosa, adenomas and carcinomas. *Clin. Exp. Immunol.* **111**, 477–483
714 (1998).
715 46. R. Peuß, *et al.*, Single cell analysis reveals modified hematopoietic cell composition
716 affecting inflammatory and immunopathological responses in Astyanax
717 mexicanus *bioRxiv*, 647255 (2019).
718 47. M. R. Riddle, *et al.*, Genetic architecture underlying changes in carotenoid
719 accumulation during the evolution of the Blind Mexican cavefish,
720 Astyanax mexicanus *bioRxiv*, 788844 (2019).
721 48. Mezquita, Mezquita, Two Opposing Faces of Retinoic Acid: Induction of Stemness or
722 Induction of Differentiation Depending on Cell-Type. *Biomolecules* **9**, 567 (2019).
723 49. P. Czarnewski, S. Das, S. Parigi, E. Villablanca, Retinoic Acid and Its Role in
724 Modulating Intestinal Innate Immunity. *Nutrients* **9**, 68 (2017).
725 50. P. Karpowicz, Y. Zhang, J. B. Hogenesch, P. Emery, N. Perrimon, The Circadian Clock
726 Gates the Intestinal Stem Cell Regenerative State. *Cell Rep.* **3**, 996–1004 (2013).
727 51. K. Parasram, P. Karpowicz, Time after time: circadian clock regulation of intestinal
728 stem cells. *Cell. Mol. Life Sci.* (2019) https:/doi.org/10.1007/s00018-019-03323-x.
729 52. E. Peyric, H. A. Moore, D. Whitmore, Circadian Clock Regulation of the Cell Cycle in
730 the Zebrafish Intestine. *PLoS One* **8**, e73209 (2013).
731 53. A. Beale, *et al.*, Circadian rhythms in Mexican blind cavefish Astyanax mexicanus in
732 the lab and in the field. *Nat. Commun.* **4**, 2769 (2013).
733 54. I. A. Frøland Steindal, A. D. Beale, Y. Yamamoto, D. Whitmore, Development of the
734 Astyanax mexicanus circadian clock and non-visual light responses. *Dev. Biol.* **441**,
735 345–354 (2018).
736 55. E. R. Duboué, A. C. Keene, R. L. Borowsky, Evolutionary convergence on sleep loss in
737 cavefish populations. *Curr. Biol.* **21**, 671–676 (2011).
738 56. Y. Elipot, L. Legendre, S. Père, F. Sohm, S. Rétaux, *Astyanax* Transgenesis and

739 Husbandry: How Cavefish Enters the Laboratory. *Zebrafish* **11**, 291–299 (2014).
740 57. R-core-team, R: A Language and Environment for Statistical Computing (2019).
741 58. C. T. Rueden, *et al.*, ImageJ2: ImageJ for the next generation of scientific image data.
742 *BMC Bioinformatics* **18** (2017).
743 59. J. M. Catchen, A. Amores, P. Hohenlohe, W. Cresko, J. H. Postlethwait, Stacks: building
744 and genotyping Loci de novo from short-read sequences. *G3 (Bethesda).* **1**, 171–82
745 (2011).
746 60. B. Langmead, S. L. Salzberg, Fast gapped-read alignment with Bowtie 2. *Nat. Methods*
747 **9**, 357–9 (2012).
748 61. D. Arends, P. Prins, R. C. Jansen, K. W. Broman, R/qtl: high-throughput multiple QTL
749 mapping: Fig. 1. *Bioinformatics* **26**, 2990–2992 (2010).
750 62. K. F. Kavalco, L. F. De Almeida-Toledo, Molecular Cytogenetics of Blind Mexican Tetra
751 and Comments on the Karyotypic Characteristics of Genus Astyanax (Teleostei,
752 Characidae). *Zebrafish* **4**, 103–111 (2007).
753 63. P. Danecek, *et al.*, The variant call format and VCFtools. *Bioinformatics* **27**, 2156–
754 2158 (2011).
755 64. M. I. Fariello, S. Boitard, H. Naya, M. SanCristobal, B. Servin, Detecting Signatures of
756 Selection Through Haplotype Differentiation Among Hierarchically Structured
757 Populations. *Genetics* **193**, 929–941 (2013).
758 65. A. Dobin, *et al.*, STAR: ultrafast universal RNA-seq aligner. *Bioinformatics* **29**, 15–21
759 (2013).
760 66. F. García-Alcalde, *et al.*, Qualimap: evaluating next-generation sequencing alignment
761 data. *Bioinformatics* **28**, 2678–2679 (2012).
762 67. Y. Liao, G. K. Smyth, W. Shi, featureCounts: an efficient general purpose program for
763 assigning sequence reads to genomic features. *Bioinformatics* **30**, 923–930 (2014).
764 68. N. Bray, H. Pimentel, P. Melsted, L. Pachter, Near-optimal RNA-Seq quantification.
765 *bioRxiv* (2015) https:/doi.org/10.1101/021592.
766 69. C. Soneson, M. I. Love, M. D. Robinson, Differential analyses for RNA-seq: transcript-
767 level estimates improve gene-level inferences. *F1000Research* **4**, 1521 (2016).
768 70. C. Soneson, M. I. Love, M. D. Robinson, Differential analyses for RNA-seq: transcript-
769 level estimates improve gene-level inferences. *F1000Research* **4**, 1521 (2015).

770 71. M. I. Love, W. Huber, S. Anders, Moderated estimation of fold change and dispersion
771 for RNA-seq data with DESeq2. *Genome Biol.* **15**, 550 (2014).
772
773

Tables

Table 1. Location of QTL markers defining confidence internal for relative hindgut length

marker	LOD	LG: position	Scaffold: position	Chromosome: position
r70838	1.64	10: 61.11	KB871783: 144963	14: 27137229
r172341	4.82	10: 68.28	KB882083: 490666	14: 17061465
r171715	2.82	10: 70.29	KB882083: 2674927	14: 11724563

Genome-wide maximum penalized LOD score using 1000 random permutations, position on the linkage group (LG), Pachón genome scaffold, and surface fish chromosome.

Table 2. Population metrics for genes in the hindgut QTL that exhibit evidence of non-neutral evolution comparing Río Choy with Tinaja

		Compared to Río Choy (n=9)						Compared to Rascón (n=8)					
		Tinaja (n=10)		Pachón (n=10)		Molino (n=9)		Tinaja (n=10)		Pachón (n=10)		Molino (n=9)	
gene ID	**gene name, description**	fixed/total alleles used	Dxy (max 21837)	fixed/total alleles used	Dxy (max 21457)	fixed/total alleles used	Dxy (Max 20517)	fixed/total alleles used	Dxy (max 20328)	fixed/total alleles used	Dxy (Max 19682)	fixed/total alleles used	Dxy (Max 18007)
ENSAMXG00000007196	cfb1, complement activation	**2/66**	**20616**	**2/65**	**20343**	0/35	19153	**3/27**	**19158**	**6/29**	**18552**	18/41	16986
ENSAMXG00000007167	cfb2, complement activation	**6/40**	**20301**	**1/34**	**17327**	0/26	13357	**1/27**	**18979**	**3/28**	**15532**	6/31	15620
ENSAMXG00000007054	rbmx2, RNA binding motif protein, X-linked 2	**1/8**	**19816**	0/7	18688	**2/7**	**18804**	NA	231	**1/1**	**5980**	**4/4**	**15183**
ENSAMXG00000007360	prdx5, peroxiredoxin 5	**2/66**	**19746**	**2/6**	**19516**	0/3	4557	NA	NA	NA	NA	3/3	15431
ENSAMXG00000007379	adssl, adenylosuccinate synthase like	**4/15**	**18587**	**5/14**	**18455**	0/9	2290	0/11	10256	**1/11**	**9232**	5/16	15065
ENSAMXG00000007093	klf5l, Kruppel-like factor 5-like	**2/8**	**17219**	0/6	3676	0/4	3755	0/6	15383	0/6	7873	0/5	4384
ENSAMXG00000007382	rce1b, Ras converting CAAX endopeptidase 1b	**1/11**	**16658**	3/12	18226	1/4	14767	0/10	15380	**1/9**	**15944**	**2/7**	**12419**
ENSAMXG00000025173	RNA-binding protein lark-like	**2/6**	**12077**	**3/6**	**15675**	**2/5**	**11921**	0/2	931	**1/2**	**4971**	**4/5**	**14059**
ENSAMXG00000007446	TENM2, teneurin transmembrane protein 2	**4/46**	**10278**	**5/44**	**10039**	**8/30**	**11529**	0/14	2628	**1/15**	**2195**	**8/21**	**3533**
ENSAMXG00000007073	slc25a14, solute carrier family	**1/5**	**10190**	0/4	6696	**0/3**	**4454**	0/3	3595	**2/5**	**15257**	1/4	7264

For each gene, the number of alleles that have fixed differences out of the total sites used, and divergence (Dxy) between the indicated surface and cave population is shown. Values in bold indicate that the genome-wide estimation of the hapFLK statistic resulted in at least one p-value less than 0.05.

Table S1. Genes within the hindgut QTL 1.5-LOD support interval that are differentially expressed in the hindgut

		Average normalized expression count				
gene stable ID	**gene name, description**	**Tinaja**	**surface**	**hybrid**	**lr**	**pw**
ENSAMXG00000006912	ubiquitin interaction motif containing 1	**641.226**	298.488	525.200	*	*
ENSAMXG00000009311	h2afy, H2A histone family member Y	**433.354**	252.691	387.330	*	*
ENSAMXG00000007120	amot, Angiomotin	**396.543**	168.257	269.468	*	*
ENSAMXG00000014597	notch1a	**106.556**	54.248	40.240	*	
ENSAMXG00000037919	plac8l1, PLAC8-like 1	**104.402**	44.104	70.487	*	*
ENSAMXG00000034188	NA	**93.520**	19.000	24.367	*	*
ENSAMXG00000018167	ERMP1, endoplasmic reticulum metallopeptidase 1	**77.677**	41.809	56.172	*	*
ENSAMXG00000019610	f2rl1.1, coagulation factor II (thrombin) receptor-like 1	**56.584**	14.651	31.024	*	*
ENSAMXG00000043097	NA	**30.063**	3.306	17.268	*	*
ENSAMXG00000040346	NA	**22.600**	0.968	1.520	*	
ENSAMXG00000030011	NA	**22.139**	0.220	8.351	*	*
ENSAMXG00000007196	cfb1, complement factor B-like	**60.433**	36.832	56.506		*
ENSAMXG00000009861	cingulin-like protein 1	**589.163**	1125.543	461.148		*
ENSAMXG00000006854	grk6, G protein-coupled receptor kinase 6	**66.554**	46.243	54.880		*
ENSAMXG00000043097	NA	**30.063**	3.306	17.268		*
ENSAMXG00000017243	ubtd2, ubiquitin domain containing 2	**27.857**	13.419	15.001		*
ENSAMXG00000040346	NA	**22.600**	0.968	1.520		*
ENSAMXG00000032351	NA	**0.869**	20.972	0.418		*
ENSAMXG00000000826	arf-GAP with Rho-GAP domain, ANK repeat and PH domain-containing	436.604	630.912	**738.131**	*	*
ENSAMXG00000037917	txnl1, thioredoxin-like 1	259.679	321.669	**382.788**	*	
ENSAMXG00000000836	reticulon, reticulon-3-A-like	3.765	174.850	**268.463**	*	*
ENSAMXG00000014252	chchd10, coiled-coil-helix-coiled-coil-helix domain containing 10	160.164	121.477	**231.895**	*	
ENSAMXG00000042179	cmc4, C-x(9)-C motif containing 4 homolog	26.142	**28.869**	48.263	*	
ENSAMXG00000043642	pgrmc1, progesterone receptor membrane component 1	1126.239	**2175.765**	1955.909	*	*
ENSAMXG00000014522	lrrc8aa, leucine rich repeat containing 8 VRAC subunit Aa	794.214	**1434.929**	1221.255	*	*
ENSAMXG00000009861	cingulin-like protein 1	589.163	**1125.543**	461.148	*	
ENSAMXG00000031422	thioredoxin domain containing 15	348.453	**541.287**	423.549	*	*
ENSAMXG00000033220	cox7b, cytochrome c oxidase subunit 7B	280.756	**415.961**	396.242	*	*
ENSAMXG00000041114	NA	24.135	**414.594**	48.999	*	*
ENSAMXG00000040749	bada, BCL2 associated agonist of cell death a	190.098	**317.216**	305.060	*	*
ENSAMXG00000037990	NA	38.642	**237.678**	230.671	*	*
ENSAMXG00000017290	rars, arginyl-tRNA synthetase	190.139	**236.984**	153.839	*	
ENSAMXG00000031420	sosondowah ankyrin repeat domain family member B	60.483	**179.482**	114.594	*	*
ENSAMXG00000034277	NLR family CARD domain-containing protein 3-like	32.671	**167.225**	48.911	*	*
ENSAMXG00000008478	kif20a, kinesin family member 20A	28.861	**146.302**	69.886	*	*
ENSAMXG00000000841	GALNT10, polypeptide N-acetylgalactosaminyltransferase 10	91.798	**138.911**	103.782	*	*
ENSAMXG00000007080	pof1b, actin binding protein	86.944	**133.568**	59.637	*	
ENSAMXG00000007243	rin1a, Ras and Rab interactor 1a	85.462	**129.130**	92.142		*
ENSAMXG00000018210	TMEM38B, transmembrane protein 38B	1718.867	**3347.577**	3040.203		*
ENSAMXG00000041114	NA	24.135	**414.594**	48.999		*

For each gene, values in bold are highest expression across sample types. Underlined values indicate the lowest expression in the F1 hybrid samples. Asterisks indicate significant difference by likelihood ratio test between all three sample types (lr) and pairwise comparison between surface fish and Tinaja cavefish (pw).

Table S2. Differentially expressed hindgut genes exhibiting highest expression in the F1 hybrid (Group 3, Figure S1)

gene stable ID	gene name	description
ENSAMXG00000000542	gys1	glycogen synthase 1 (muscle) [Source:ZFIN;Acc:ZDB-GENE-040426-1243]
ENSAMXG00000003217		NULL
ENSAMXG00000003528	ITLN1 (1 of many)	intelectin 1 [Source:HGNC Symbol;Acc:HGNC:18259]
ENSAMXG00000005979	timeless	timeless circadian clock [Source:ZFIN;Acc:ZDB-GENE-030131-8978]
ENSAMXG00000006267	esr1	estrogen receptor 1 [Source:ZFIN;Acc:ZDB-GENE-020806-5]
ENSAMXG00000006712	caskin1	CASK interacting protein 1 [Source:ZFIN;Acc:ZDB-GENE-071115-3]
ENSAMXG00000008593	pir	pirin [Source:ZFIN;Acc:ZDB-GENE-040718-288]
ENSAMXG00000009578	adcy8	adenylate cyclase 8 (brain) [Source:ZFIN;Acc:ZDB-GENE-070912-197]
ENSAMXG00000011826	si:ch211-132f19.7	si:ch211-132f19.7 [Source:ZFIN;Acc:ZDB-GENE-130530-619]
ENSAMXG00000011960	cyp26a1	cytochrome P450, family 26, subfamily A, polypeptide 1 [Source:ZFIN;Acc:ZDB-GENE-990415-44]
ENSAMXG00000012719		heat shock 70 kDa protein 12A-like [Source:NCBI gene;Acc:103046531]
ENSAMXG00000013859	glsa	glutaminase a [Source:ZFIN;Acc:ZDB-GENE-050204-3]
ENSAMXG00000014779	sgsm3	small G protein signaling modulator 3 [Source:ZFIN;Acc:ZDB-GENE-040426-2635]
ENSAMXG00000014901	apeh	acylaminoacyl-peptide hydrolase [Source:ZFIN;Acc:ZDB-GENE-030131-9870]
ENSAMXG00000015029	rorcb	RAR-related orphan receptor C b [Source:ZFIN;Acc:ZDB-GENE-040724-215]
ENSAMXG00000018475		NULL
ENSAMXG00000018995		peroxiredoxin-1 [Source:NCBI gene;Acc:103031813]
ENSAMXG00000019373	nudcd3	NudC domain containing 3 [Source:ZFIN;Acc:ZDB-GENE-040426-2255]
ENSAMXG00000019396	cygb1	cytoglobin 1 [Source:ZFIN;Acc:ZDB-GENE-020513-1]
ENSAMXG00000020744	c8g	complement component 8, gamma polypeptide [Source:ZFIN;Acc:ZDB-GENE-040426-1898]
ENSAMXG00000021464	si:ch211-276a23.5	si:ch211-276a23.5 [Source:ZFIN;Acc:ZDB-GENE-141215-4]
ENSAMXG00000024777	eno1a	enolase 1a, (alpha) [Source:ZFIN;Acc:ZDB-GENE-030131-6048]
ENSAMXG00000024896	nrarpa	NOTCH regulated ankyrin repeat protein a [Source:ZFIN;Acc:ZDB-GENE-030515-6]
ENSAMXG00000025981		NULL
ENSAMXG00000027124	RF00478	NULL
ENSAMXG00000029674	trh	thyrotropin-releasing hormone [Source:ZFIN;Acc:ZDB-GENE-020930-1]
ENSAMXG00000030396	mb	myoglobin [Source:ZFIN;Acc:ZDB-GENE-040426-1430]
ENSAMXG00000031413		solute carrier family 22 member 4-like [Source:NCBI gene;Acc:103029834]
ENSAMXG00000031569	vrk3	vaccinia related kinase 3 [Source:ZFIN;Acc:ZDB-GENE-030131-246]
ENSAMXG00000031818	zgc:92606	zgc:92606 [Source:ZFIN;Acc:ZDB-GENE-040718-462]
ENSAMXG00000034120	slc29a3	solute carrier family 29 (equilibrative nucleoside transporter), member 3 [Source:ZFIN;Acc:ZDB-GENE-081107-66]
ENSAMXG00000034331		NULL
ENSAMXG00000035277	zdhhc11	zinc finger, DHHC-type containing 11 [Source:ZFIN;Acc:ZDB-GENE-130530-795]
ENSAMXG00000035722		NULL
ENSAMXG00000036341	hexb	hexosaminidase B (beta polypeptide) [Source:ZFIN;Acc:ZDB-GENE-030131-2333]
ENSAMXG00000036770	fhdc4	FH2 domain containing 4 [Source:ZFIN;Acc:ZDB-GENE-131127-25]
ENSAMXG00000037811	SECISBP2L	SECIS binding protein 2 like [Source:HGNC Symbol;Acc:HGNC:28997]
ENSAMXG00000038275		NULL
ENSAMXG00000038302		NULL
ENSAMXG00000038552	CASQ2	calsequestrin 2 [Source:HGNC Symbol;Acc:HGNC:1513]
ENSAMXG00000038579		NULL
ENSAMXG00000039496		NULL
ENSAMXG00000040338		intelectin-like [Source:NCBI gene;Acc:103036009]
ENSAMXG00000041228		NULL
ENSAMXG00000041671	wipi1	WD repeat domain, phosphoinositide interacting 1 [Source:ZFIN;Acc:ZDB-GENE-040426-1404]
ENSAMXG00000041918	guca1c	guanylate cyclase activator 1C [Source:ZFIN;Acc:ZDB-GENE-030829-1]
ENSAMXG00000041920	slc1a2b	solute carrier family 1 (glial high affinity glutamate transporter), member 2b [Source:ZFIN;Acc:ZDB-GENE-030131-7779]
ENSAMXG00000042050		NULL
ENSAMXG00000042163		NULL
ENSAMXG00000042450	ankrd46a	ankyrin repeat domain 46a [Source:ZFIN;Acc:ZDB-GENE-030131-2643]
ENSAMXG00000042617	plpp1a	phospholipid phosphatase 1a [Source:ZFIN;Acc:ZDB-GENE-080225-26]
ENSAMXG00000042843	rdh1	retinol dehydrogenase 1 [Source:ZFIN;Acc:ZDB-GENE-030912-15]
ENSAMXG00000042921	PSMB11 (1 of many)	proteasome subunit beta 11 [Source:HGNC Symbol;Acc:HGNC:31963]
ENSAMXG00000043019		NULL
ENSAMXG00000044068		NULL

Table S2. Differentially expressed hindgut genes exhibiting lowest expression in the F1 hybrid (Group 4, Figure S1)

gene stable ID	gene name	description
ENSAMXG00000001449	mat2al	methionine adenosyltransferase II, alpha-like [Source:ZFIN;Acc:ZDB-GENE-060421-5255]
ENSAMXG00000002813		NULL
ENSAMXG00000004203	dock3	dedicator of cytokinesis 3 [Source:ZFIN;Acc:ZDB-GENE-100624-1]
ENSAMXG00000004229	gdpd1	glycerophosphodiester phosphodiesterase domain containing 1 [Source:ZFIN;Acc:ZDB-GENE-040822-22]
ENSAMXG00000004732	bag3	BCL2 associated athanogene 3 [Source:ZFIN;Acc:ZDB-GENE-040801-40]
ENSAMXG00000005293	evplb	envoplakin b [Source:ZFIN;Acc:ZDB-GENE-030131-212]
ENSAMXG00000007764	krt1-c5	keratin, type 1, gene c5 [Source:ZFIN;Acc:ZDB-GENE-060316-3]
ENSAMXG00000009861		cingulin-like protein 1 [Source:NCBI gene;Acc:103022577]
ENSAMXG00000010263	CASP6	caspase 6 [Source:HGNC Symbol;Acc:HGNC:1507]
ENSAMXG00000010610	ppl	periplakin [Source:ZFIN;Acc:ZDB-GENE-041008-196]
ENSAMXG00000011397	spire1a	spire-type actin nucleation factor 1a [Source:ZFIN;Acc:ZDB-GENE-061013-119]
ENSAMXG00000011672	slc9a3r1a	solute carrier family 9, subfamily A (NHE3, cation proton antiporter 3), member 3 regulator 1a [Source:ZFIN;Acc:ZDB-GENE-031006-7]
ENSAMXG00000011790	zgc:172079	zgc:172079 [Source:ZFIN;Acc:ZDB-GENE-080204-103]
ENSAMXG00000012301	slc4a4a	solute carrier family 4 (sodium bicarbonate cotransporter), member 4a [Source:ZFIN;Acc:ZDB-GENE-060526-274]
ENSAMXG00000013027	brca2	breast cancer 2, early onset [Source:ZFIN;Acc:ZDB-GENE-060510-3]
ENSAMXG00000013552	pabpc1l	poly(A) binding protein, cytoplasmic 1-like [Source:ZFIN;Acc:ZDB-GENE-030131-5836]
ENSAMXG00000013796	pak1	p21 protein (Cdc42/Rac)-activated kinase 1 [Source:ZFIN;Acc:ZDB-GENE-030826-29]
ENSAMXG00000015091		NULL
ENSAMXG00000015951	eps8l2	EPS8 like 2 [Source:ZFIN;Acc:ZDB-GENE-131121-340]
ENSAMXG00000017060	galnt7	UDP-N-acetyl-alpha-D-galactosamine: polypeptide N-acetylgalactosaminyltransferase 7 [Source:ZFIN;Acc:ZDB-GENE-050522-284]
ENSAMXG00000017336	slc5a1 (1 of many)	solute carrier family 5 (sodium/glucose cotransporter), member 1 [Source:ZFIN;Acc:ZDB-GENE-040426-1524]
ENSAMXG00000017464	lmo7a	LIM domain 7a [Source:ZFIN;Acc:ZDB-GENE-030219-74]
ENSAMXG00000017536		polypeptide N-acetylgalactosaminyltransferase 6-like [Source:NCBI gene;Acc:103034470]
ENSAMXG00000017853		transmembrane protease serine 9-like [Source:NCBI gene;Acc:103044070]
ENSAMXG00000018625	per1b	period circadian clock 1b [Source:ZFIN;Acc:ZDB-GENE-040419-1]
ENSAMXG00000021143	slc7a8a	solute carrier family 7 (amino acid transporter light chain, L system), member 8a [Source:ZFIN;Acc:ZDB-GENE-121120-2]
ENSAMXG00000025148	STX19	syntaxin 19 [Source:HGNC Symbol;Acc:HGNC:19300]
ENSAMXG00000029238	si:ch211-137i24.10	si:ch211-137i24.10 [Source:ZFIN;Acc:ZDB-GENE-060526-34]
ENSAMXG00000029616	ugt5d1 (1 of many)	UDP glucuronosyltransferase 5 family, polypeptide D1 [Source:ZFIN;Acc:ZDB-GENE-091118-36]
ENSAMXG00000029919	b3gnt3.4	UDP-GlcNAc:betaGal beta-1,3-N-acetylglucosaminyltransferase 3, tandem duplicate 4 [Source:ZFIN;Acc:ZDB-GENE-030131-8875]
ENSAMXG00000029933		annexin A2-like [Source:NCBI gene;Acc:103024979]
ENSAMXG00000030052	pcbd1	pterin-4 alpha-carbinolamine dehydratase/dimerization cofactor of hepatocyte nuclear factor 1 alpha [Source:ZFIN;Acc:ZDB-GENE-040426-1787]
ENSAMXG00000031773		NULL
ENSAMXG00000032507		zinc finger protein 800-like [Source:NCBI gene;Acc:103026180]
ENSAMXG00000033111		NULL
ENSAMXG00000033217		NULL
ENSAMXG00000033692		NULL
ENSAMXG00000034400		NULL
ENSAMXG00000036383		suppressor of cytokine signaling 2-like [Source:NCBI gene;Acc:111191435]
ENSAMXG00000036963		cerebellin-2-like [Source:NCBI gene;Acc:103040140]
ENSAMXG00000037136	zgc:103681	zgc:103681 [Source:ZFIN;Acc:ZDB-GENE-041010-17]
ENSAMXG00000037535		NULL
ENSAMXG00000038262		NULL
ENSAMXG00000040014	serpinb1l2	serpin peptidase inhibitor, clade B (ovalbumin), member 1, like 2 [Source:ZFIN;Acc:ZDB-GENE-041001-117]
ENSAMXG00000040633		NULL
ENSAMXG00000040957		NULL
ENSAMXG00000041754	rtn2a	reticulon 2a [Source:ZFIN;Acc:ZDB-GENE-060420-1]
ENSAMXG00000042112	bco1	beta-carotene oxygenase 1 [Source:ZFIN;Acc:ZDB-GENE-010508-1]
ENSAMXG00000042476	slc25a15b	solute carrier family 25 (mitochondrial carrier; ornithine transporter) member 15b [Source:ZFIN;Acc:ZDB-GENE-060526-35]
ENSAMXG00000043501		voltage-gated potassium channel subunit beta-2 [Source:NCBI gene;Acc:103043691]
ENSAMXG00000043650		NULL
ENSAMXG00000043711	pparab	peroxisome proliferator-activated receptor alpha b [Source:ZFIN;Acc:ZDB-GENE-990415-211]
ENSAMXG00000043975	slc1a1	solute carrier family 1 (neuronal/epithelial high affinity glutamate transporter, system Xag), member 1 [Source:ZFIN;Acc:ZDB-GENE-040718-414]

Figures and figure legends

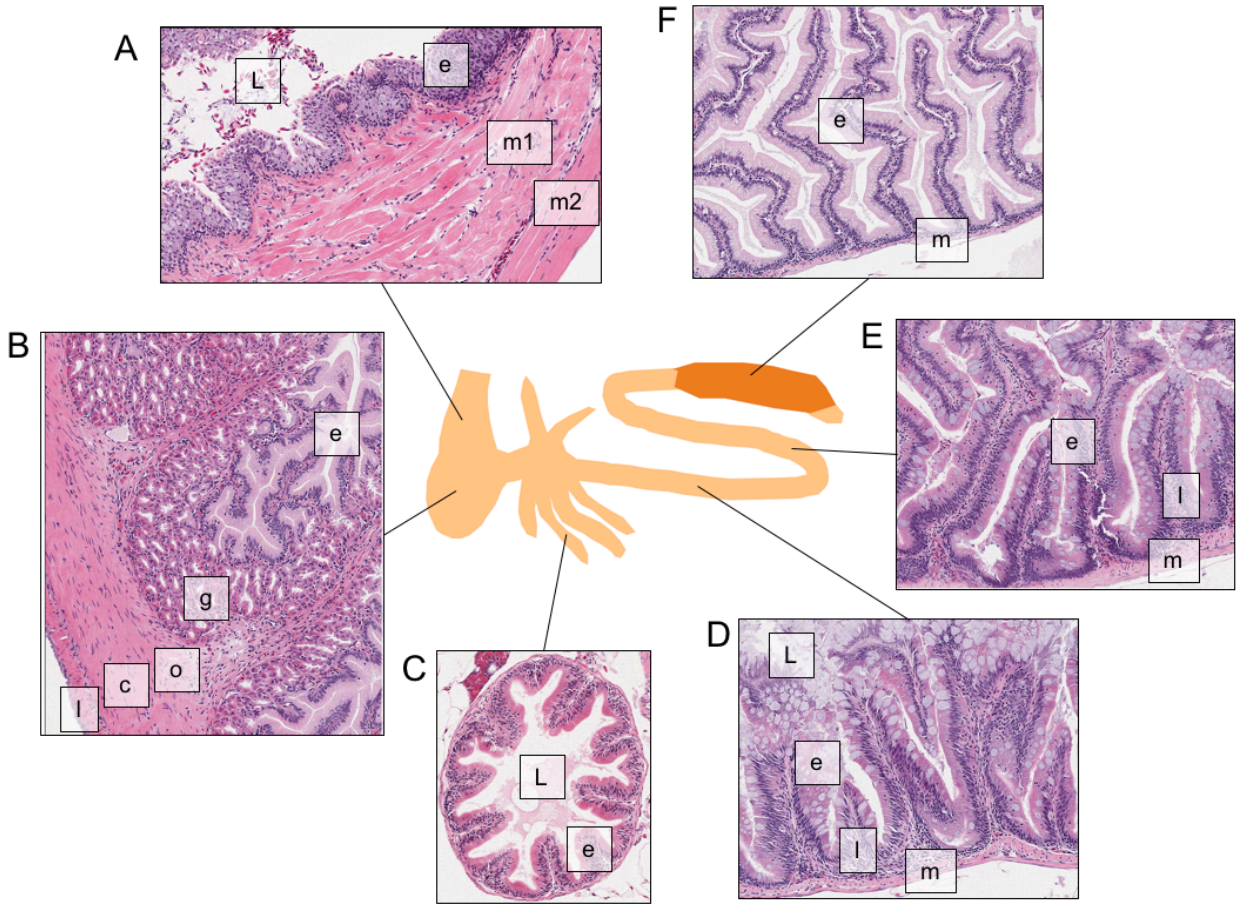

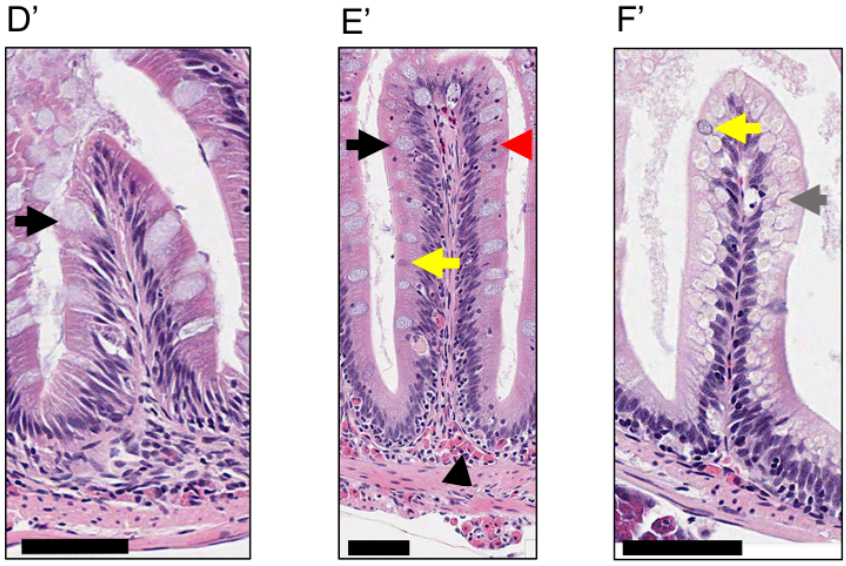

Figure 1. Histology of the *Astyanax mexicanus* surface fish gastrointestinal tract as shown by hematoxylin and eosin staining. A, Transverse section of esophageal region (L: lumen, e: epithelium, m1-2: muscle layers). B, Stomach section showing epithelium (e), eosinophilic gastric glands (g), and layers of muscle (o: orthogonal, c: circumferential, l: longitudinal). C, Cross section of a pyloric caecum showing the lumen (L) and ridged epithelium (e). D, Transverse section of the proximal midgut showing lumen filled with mucus (L), epithelium (e), lamina propria (l), and circumferential inner and longitudinal outer muscle layers (m). E, Transverse section of a more posterior section of the midgut showing epithelium (e), lamina propria (l), and circumferential inner and longitudinal outer muscle layers (m). F, Transverse section of the hindgut showing epithelium (e), and muscle layers (m). A-F image magnification is 10X. D-F' 20X images (scale bar is 50µM) showing the cell types of the gut epithelium in the proximal midgut (D'), distal midgut (E'), and hindgut (F'). Black arrows highlight the differences between secretory goblet cells in the proximal (D') and distal (E') midgut. Black arrow head in E' indicates group of immune cells (pink). Red arrow head shows pyknotic nuclei. Grey arrow in F' highlights cells with hydrophobic (mostly clear) structures within the cytoplasm. D-E are images from the same slide.

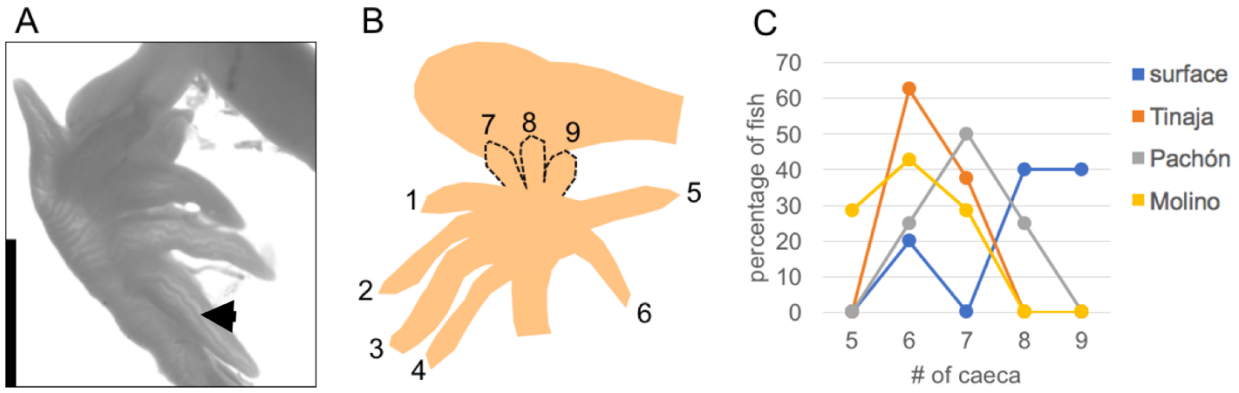

Figure 2. Pyloric caeca structure and number in *Astyanax mexicanus* surface and cave morphs. A, Image of the region of gut containing pyloric caeca. The darker lines show the ridged morphology of the epithelium (black arrow, scale bar is 2 mm). B, Drawing of the pyloric caeca indicating the position and number of caeca. The caeca at position 7, 8, and 9 are variable. C, Graph comparing percentage of one-month old fish with the indicated number of total caeca for each population (n=5, 6, 8, 6).

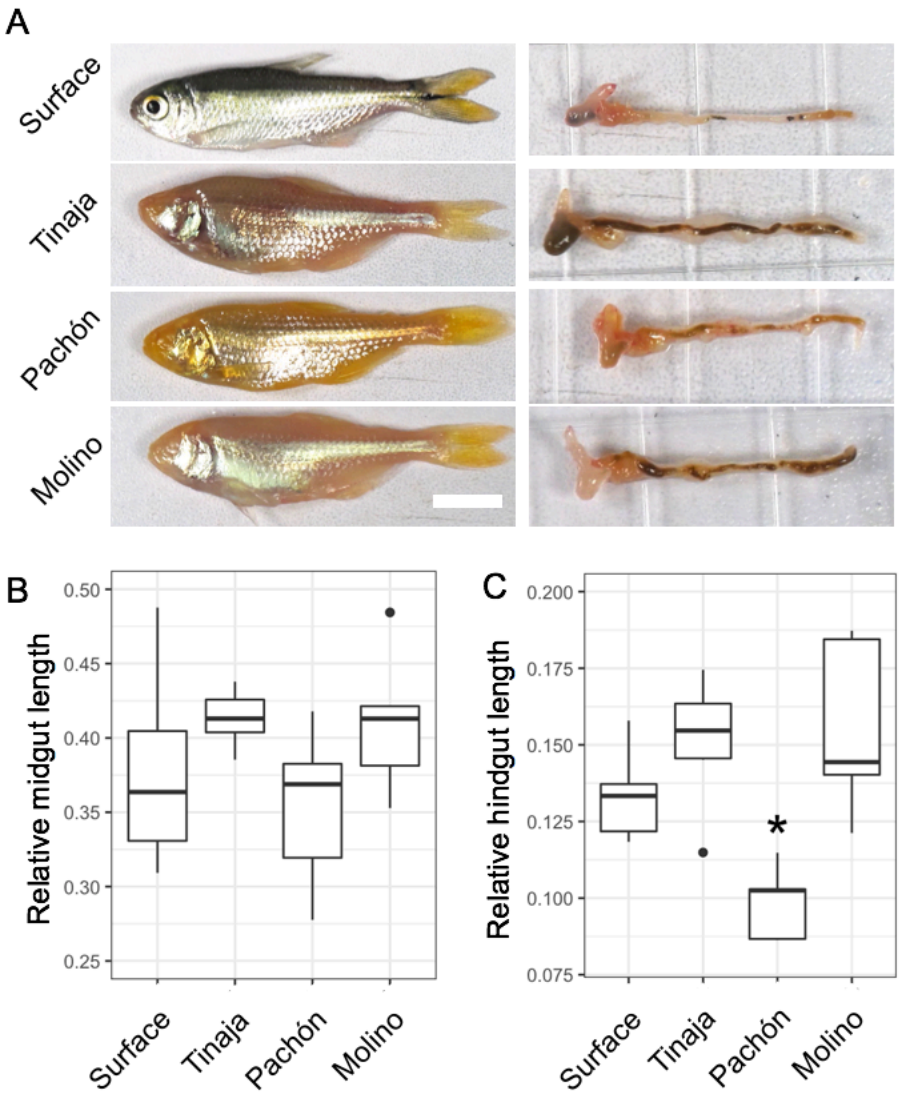

Figure 3. Relative length of the gastrointestinal (GI) tract of *Astyanax mexicanus* surface and cave morphs. A, Images of fish from the indicated populations that were fed 6 mg of pellet food per day for greater than 8 months and their GI tracts (scale bars is 1cm). B, Boxplots showing relative midgut and hindgut length of fish from the indicated populations (n=6 for surface, Tinaja, and Pachón. n=5 for Molino). For box plots, median, 25th, 50th, and 75th percentiles are represented by horizontal bars and vertical bars represent 1.5 interquartile ranges. Asterisks indicates Pachón relative hindgut length is significantly less than surface (p=0.05), Tinaja (p=0.002), and Molino (p=0.001, one-way ANOVA with Turkey's post hoc test).

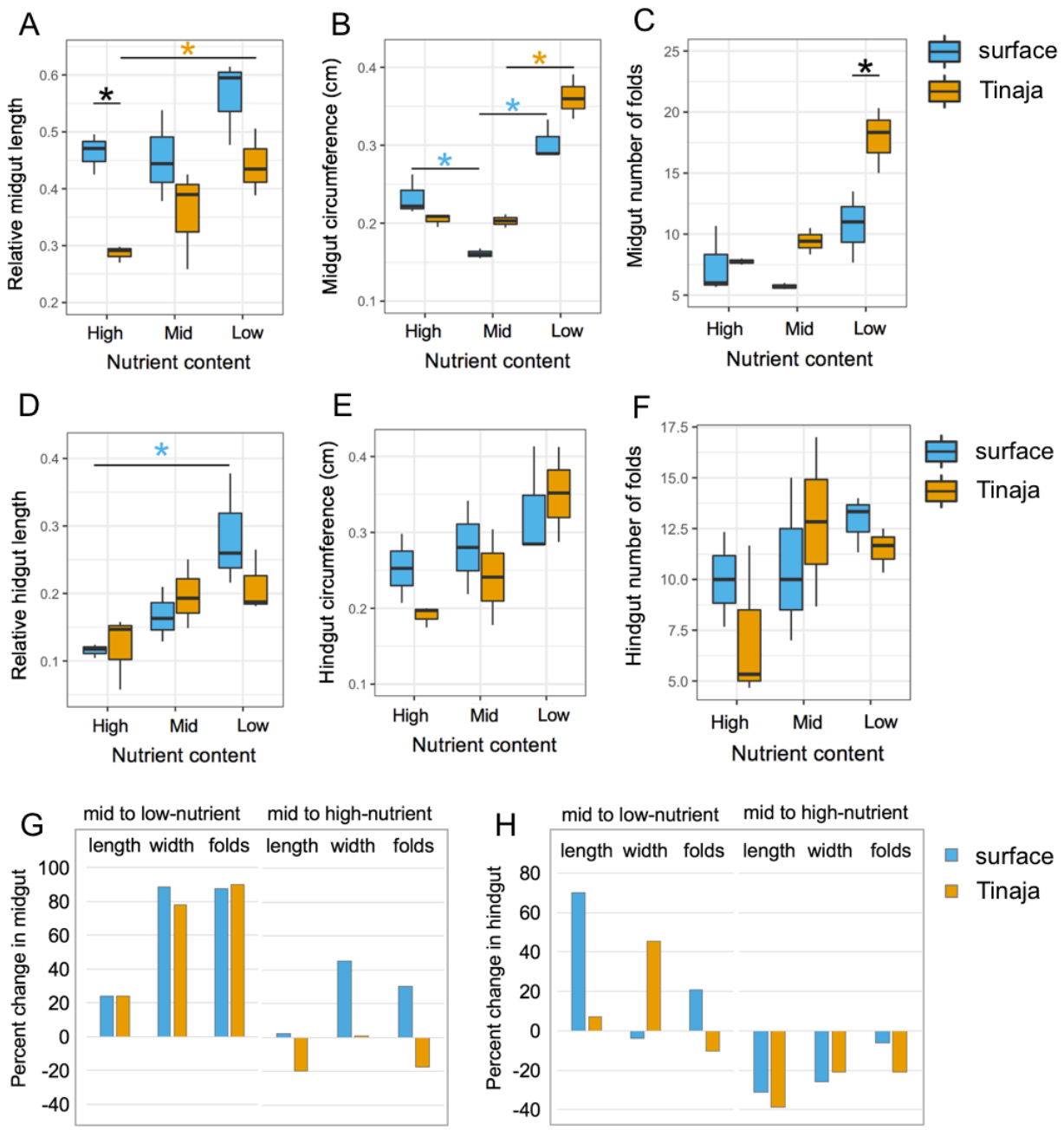

Figure 4. Diet influences *A. mexicanus* gut morphology. Relative length, circumference, and number of folds in the epithelium in the midgut (A-C) and hindgut (D-E) in fish continuously fed a moderate diet or switched to a high-nutrient or low nutrient diet as adults (n=3 fish per population and diet, and 3 tissue sections average per individual fish). In boxplots, median, 25th, 50th, and 75th percentiles are represented by horizontal bars and vertical bars represent 1.5 interquartile ranges. Significance code (*p<0.05) from one-way ANOVA with HSD post hoc test comparing between populations (black asterisks) or within population by diet (orange asterisks = Tinaja, blue asterisks = surface fish). Bar graphs show percent change in the indicated phenotype in the midgut (G) and hindgut (H).

A surface fish

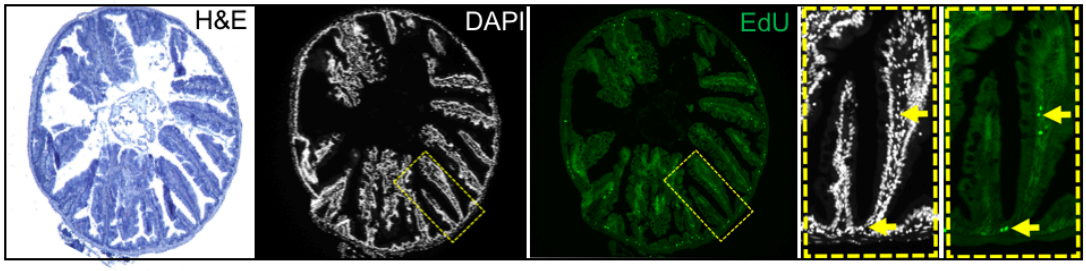

B Tinaja cavefish

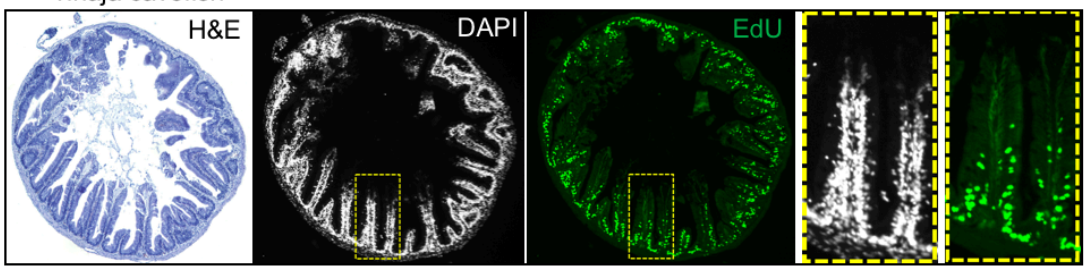

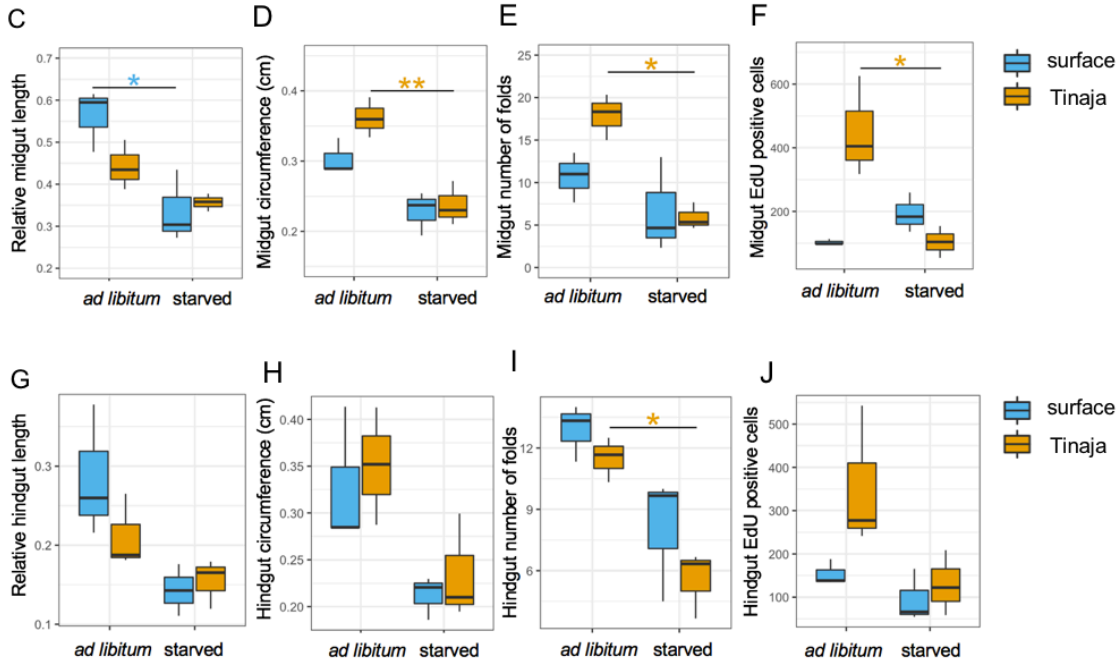

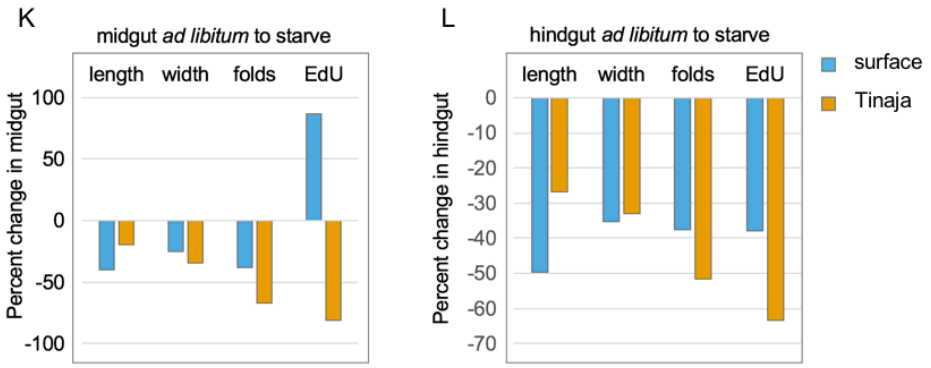

Figure 5. Cavefish have more proliferation in the intestinal epithelium on a low-nutrient diet compared to surface fish and, reduce proliferation in response to starvation. Cross section of midgut in surface fish (A) and Tinaja cavefish (B) stained with H&E (left) and serial section showing DAPI staining and EdU positive cells; larger view of yellow boxed region shown in right panels. Yellow arrows point to EdU positive cells. Note yellow arrow near the tip of the fold shows cell in the lamina propria. C-F, Quantification of midgut length, circumference, number of folds, and EdU positive cells in fish fed *ad libitum* versus starved for two weeks. G-J, Quantification of hindgut length, circumference, number of folds, and EdU positive cells in fish fed *ad libitum* versus fasted for two weeks (n=3 fish per population and diet and 3 tissue sections averaged per individual fish). In boxplots, median, 25th, 50th, and 75th percentiles are represented by horizontal bars and vertical bars represent 1.5 interquartile ranges. Significance code (*$p<0.05$, **$p<.005$) from one-way ANOVA with HSD post hoc test. K-L, Bar graphs showing percent change in the indicated phenotypes in the midgut (K) and hindgut (L).

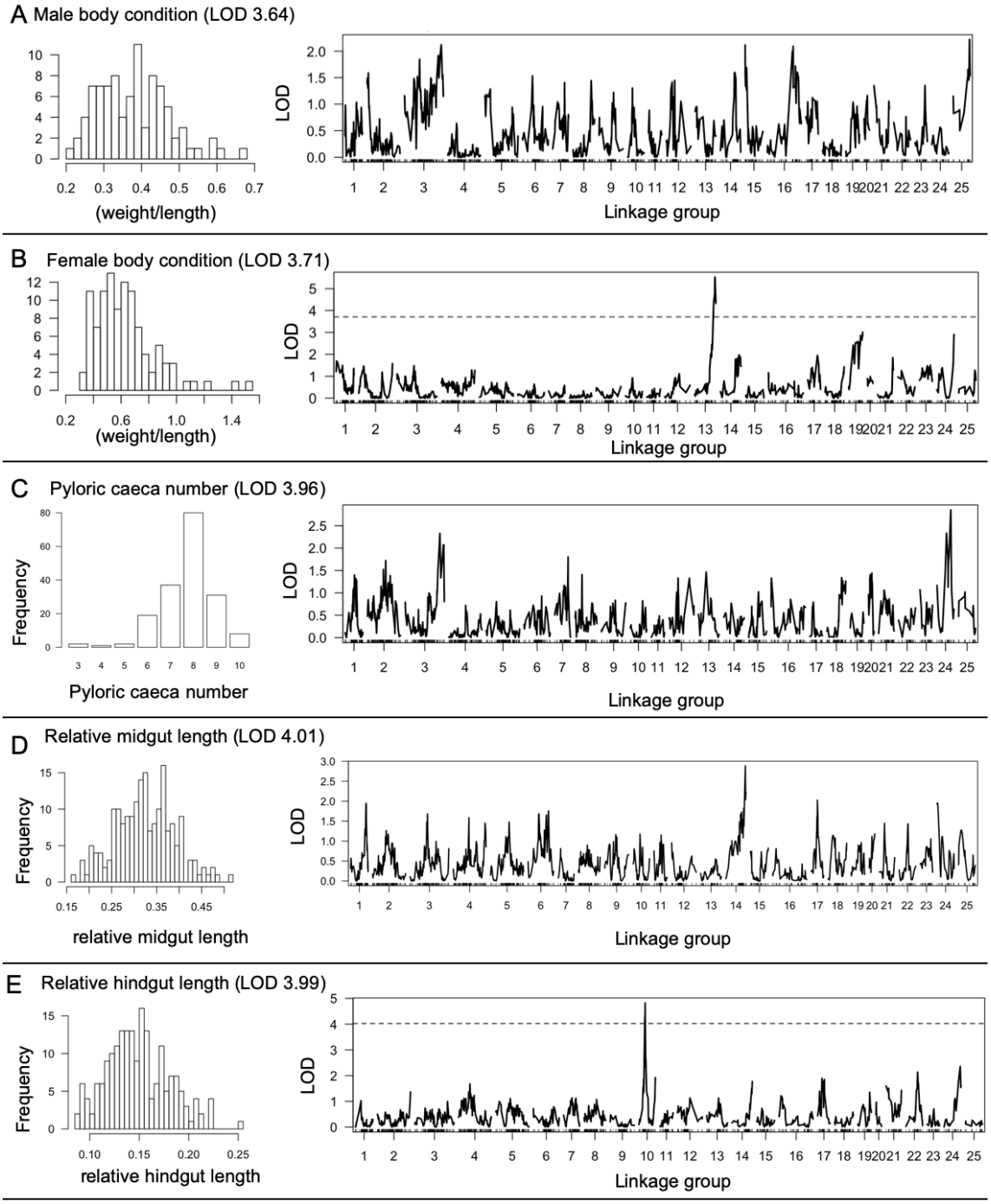

Figure 6. Genetic mapping of body condition and gut morphology in adult *A. mexicanus* surface/Tinaja F2 hybrids. A-E, Histograms showing distribution of the indicated phenotypes in F2 hybrids and (right) genome wide scan showing logarithm of the odds (LOD) score for the indicated phenotypes using Haley-Knott regression mapping. A, B non-parametric model, C-E normal model. Significance thresholds at p=0.05 are indicated in parenthesis following the phenotype.

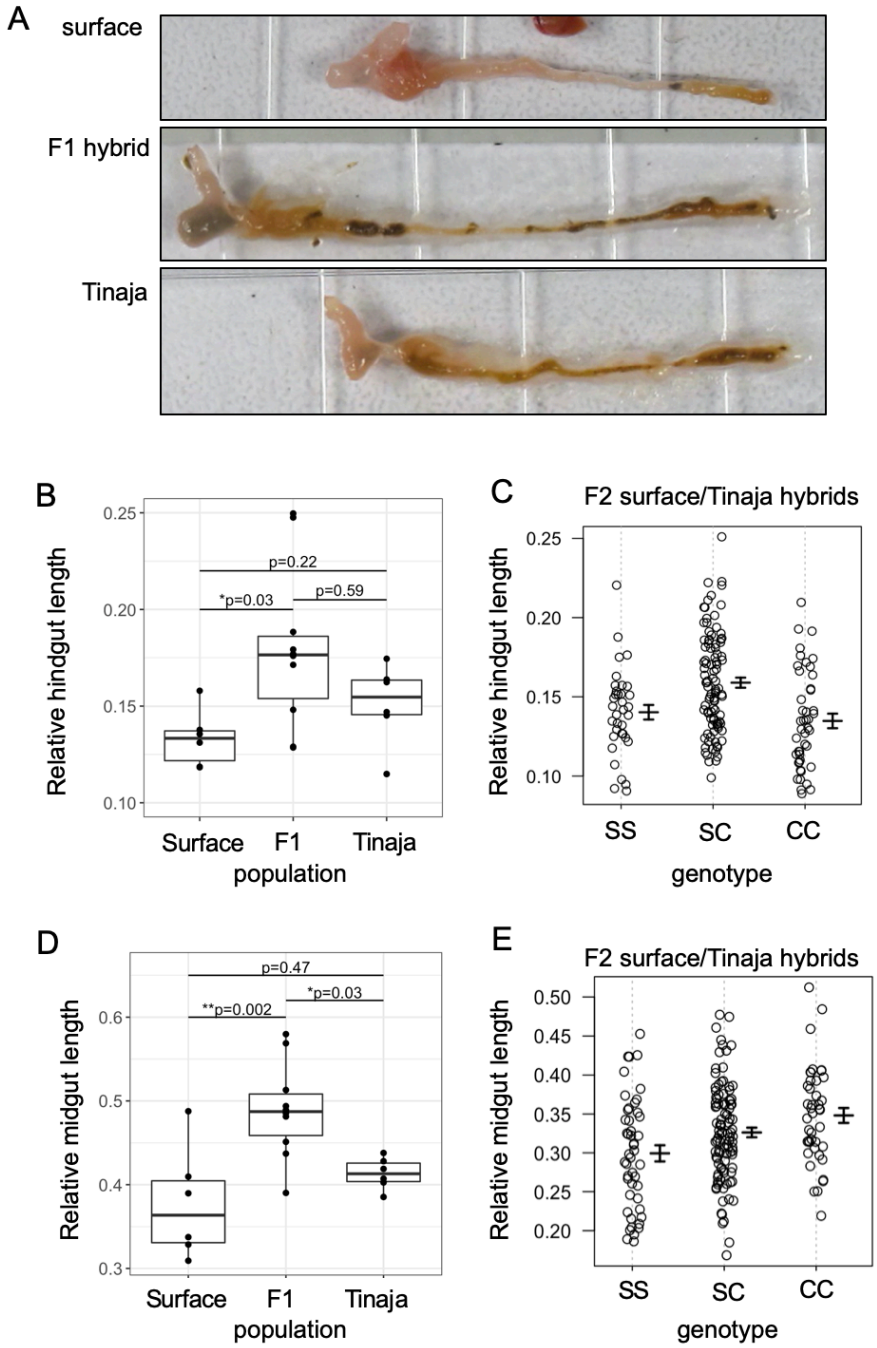

Figure 7. Gut length heterosis in surface/Tinaja hybrids. A, Image of gut from surface fish, surface/Tinaja F1 hybrid, and Tinaja cavefish of similar lengths. B, Quantification of relative hindgut length in surface (n=6), F1 hybrid (n=10), Tinaja (n=6). C, Quantification of relative hindgut length of surface/Tinaja F2 hybrids with the indicated genotype at the marker with the highest LOD score (SS: homozygous surface, SC: heterozygous, CC: homozygous cave). D, Quantification of relative midgut length in in surface (n=6), F1 hybrid (n=10), Tinaja (n=6). E, Quantification of relative midgut length of surface/Tinaja F2 hybrids with the indicated genotype at the marker with the highest LOD score (SS: homozygous surface, SC: heterozygous CC: homozygous cave).

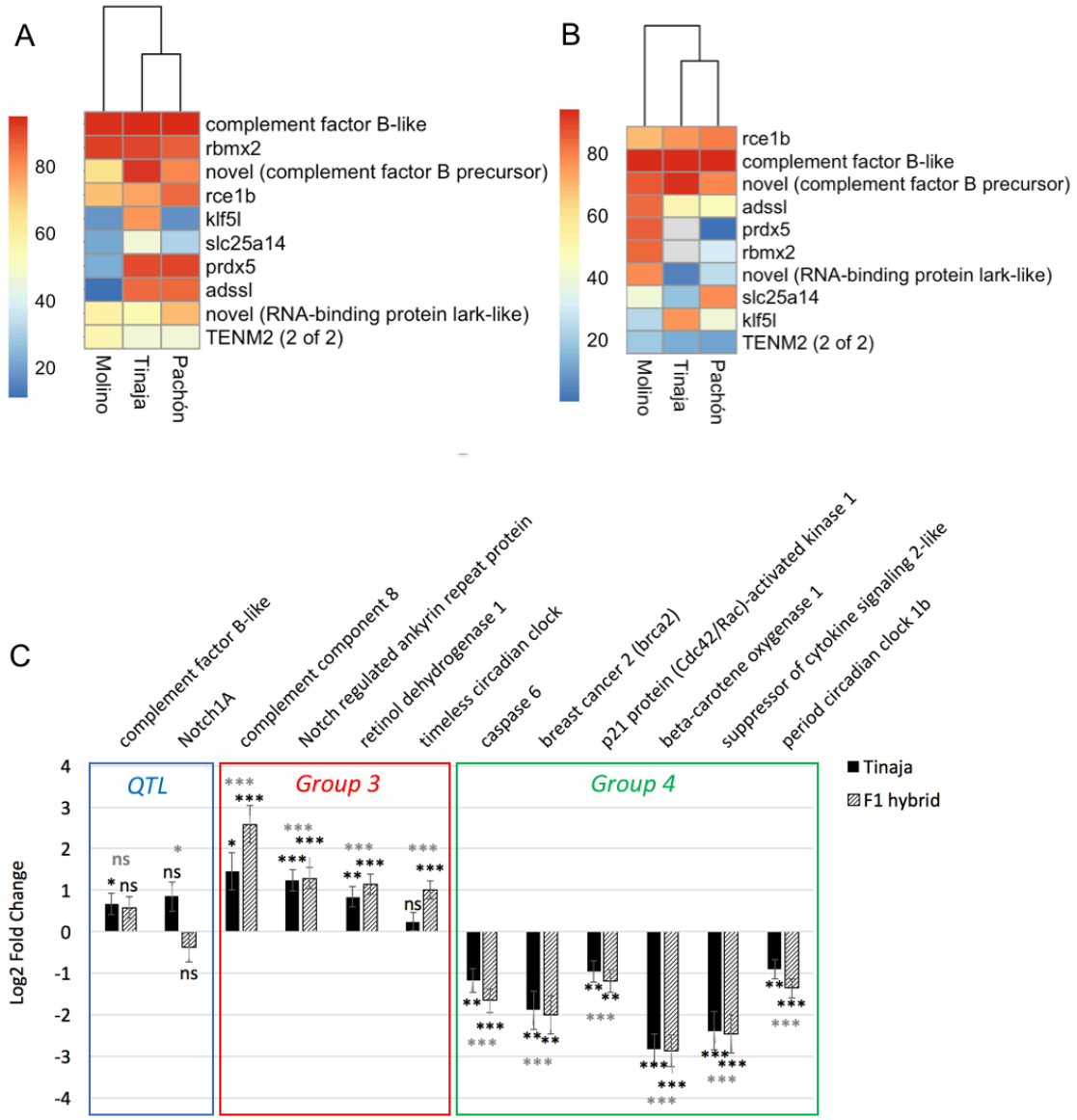

Figure 8. Population genetics and RNA sequencing analysis of candidate genes controlling hindgut length. A, B, Heat maps showing the genome-wide divergence percentile of genes within the hindgut QTL that have significant HapFLK p-values. A, Divergence of Río Choy surface fish from three cavefish populations, and B, Divergence of Rascón surface fish from three cavefish populations. C, Log2 Fold expression change compared to surface fish of a subset of genes within the hindgut QTL (blue), or that are a part of the gene cluster that shows lowest (group3, red) and highest (group4, green) expression in F1 hybrids. Grey significance codes from likelihood ratio test comparing all three sample types and black asterisks next to bars indicate significance from Wald test comparing to only surface fish (Significance code for adjusted p-value: *<.05 **<.005 ***<.0005, ns>.05). Error bars indicate standard error estimate for log2 fold change.

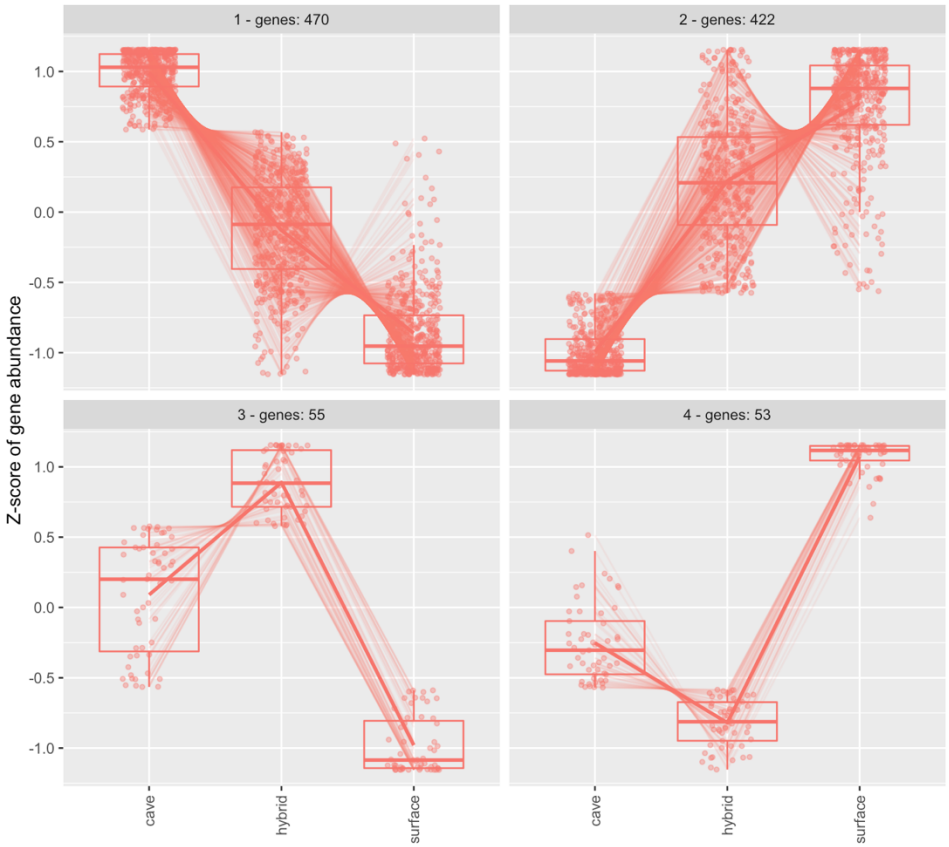

Supplemental Figure 1: Gene expression clusters of genes that are differentially expressed between Tinaja, Surface, and F1 hybrid hindguts (n=5 hindguts per population).